Feedback Microtubule Control and Microtubule-Actin Cross-talk in *Arabidopsis* Revealed by Integrative Proteomic and Cell Biology Analysis of *KATANIN 1* Mutants*[S]

Tomáš Takáč‡¶, Olga Šamajová‡¶, Tibor Pechan§, Ivan Luptovčiak‡, and Jozef Šamaj‡‖

Microtubule organization and dynamics are critical for key developmental processes such as cell division, elongation, and morphogenesis. Microtubule severing is an essential regulator of microtubules and is exclusively executed by KATANIN 1 in *Arabidopsis*. In this study, we comparatively studied the proteome-wide effects in two *KATANIN 1* mutants. Thus, shotgun proteomic analysis of roots and aerial parts of single nucleotide mutant *fra2* and T-DNA insertion mutant *ktn1-2* was carried out. We have detected 42 proteins differentially abundant in both *fra2* and *ktn1-2*. KATANIN 1 dysfunction altered the abundance of proteins involved in development, metabolism, and stress responses. The differential regulation of tubulins and microtubule-destabilizing protein MDP25 implied a feedback microtubule control in *KATANIN 1* mutants. Furthermore, deregulation of profilin 1, actin-depolymerizing factor 3, and actin 7 was observed. These findings were confirmed by immunoblotting analysis of actin and by microscopic observation of actin filaments using fluorescently labeled phalloidin. Results obtained by quantitative RT-PCR analysis revealed that changed protein abundances were not a consequence of altered expression levels of corresponding genes in the mutants. In conclusion, we show that abundances of several cytoskeletal proteins as well as organization of microtubules and the actin cytoskeleton are amended in accordance with defective microtubule severing. *Molecular & Cellular Proteomics 16: 10.1074/mcp.M117.068015, 1591–1609, 2017.*

Microtubules are tubulin filamentous polymers involved in cell division and expansion (1, 2). They are capable of rapid elongation or shortening (polymerization and depolymerization), which is known as dynamic instability. This dynamic instability together with other mechanisms, including nucleation, branching, severing, and bundling, determine the spatiotemporal organization of microtubule arrays, which is crucial for plant growth and development (3–5). Microtubule dynamics and organization are controlled mainly by microtubule-associated proteins (MAPs),[1] kinesins, plus-end binding (EB1) proteins, microtubule-severing protein katanin, microtubule-destabilizing protein 25 (MDP25), phospholipase Dα1, and others (6–8). Some of these proteins might be regulated by signaling molecules such as mitogen-activated protein kinases (9, 10), Rop GTPases, calcium, and phosphatidic acid (11–13). Such interactions couple microtubules to the external environment and mediate their developmental or conditional rearrangements.

KATANIN 1 is a microtubule-severing AAA-ATPase assembled from a catalytic subunit of 60 kDa (p60) and a structural 80-kDa subunit (p80 (14)). It is capable of severing microtubules in an ATP-dependent manner (15). At the cellular level, the severing activity of KATANIN 1 was shown to regulate plant microtubule organization (16). Except for microtubule severing, KATANIN 1 activity favors microtubule bundle formation (17) and can be modulated by other microtubule-binding proteins like SPIRAL2 (18). Moreover, KATANIN 1 severing activity is induced by Rho-GTPase signaling, thus connecting hormonal and external stimuli to microtubule dynamics (19).

From the ‡Centre of the Region Haná for Biotechnological and Agricultural Research, Faculty of Science, Palacký University, Šlechtitelů 27, 783 71 Olomouc, Czech Republic; §Institute for Genomics, Biocomputing and Biotechnology, Mississippi Agricultural and Forestry Experiment Station, Mississippi State University, Starkville, Mississippi 39759

Received February 21, 2017, and in revised form, June 6, 2017
Published, MCP Papers in Press, July 13, 2017, DOI 10.1074/mcp.M117.068015
Author contributions: J. S. designed research; T. T., O. S., T. P., and I. L. performed research; T. T., O. S., and T. P. analyzed data; T. T., O. S., and J. S. wrote the paper. All authors reviewed the manuscript.

[1] The abbreviations used are: MAP, microtubule-associated protein; ABA, abscisic acid; ABP, actin-binding protein; ADF, actin-depolymerizing factor; GA, giberellic acid; IAA, indole-3-acetic acid; MDP25, microtubule-destabilizing protein 25; TUB4, TUBULIN β-4; TSN, TUDOR-staphylococcal nuclease protein; WPP2, WPP domain-containing protein 2; FDR, false discovery rate; BSE, *m*-maleimidobenzoyl-*N*-hydroxysuccinimide ester; ANOVA, analysis of variance; PII, precursor ion intensity; M-MLV, Moloney murine leukemia virus; GO, gene ontology.

The importance of KATANIN 1 for plant development is manifested by multiple developmental defects reported in *KATANIN 1* mutants such as *fra2* or *lue1*. They exhibit reduced root, hypocotyl, stem, and leaf growth as well as stubby flower organs with reduced anther length (20–22). *KATANIN 1* mutants show reduced fertility and defects in ovule and anther development, and they exhibit aberrant embryogenesis and seed formation (23). It is generally accepted that these phenotypes are caused by reduced cell expansion (20, 21). It was also proposed that *fra2* and *lue1* mutants exhibit some defects in cell division resulting from altered organization of microtubule arrays showing multipolar spindles and disorientation of the cell division plane (24). Advanced live microscopy of microtubules in *ktn1-2* uncovered the contribution of KATANIN 1 to dynamic organization of cortical microtubules as well as a new function in the formation and maturation of preprophase band and rectification of cell division plane (25). Moreover, *KATANIN 1* mutants displayed altered gibberellic acid (GA) and ethylene responses (22, 26) pointing to the role of KATANIN 1 in controlling microtubule reorganization in response to hormones.

Integrative bioinformatics analyses of *Leishmania* flagellar genes and proteins revealed that katanin along with profilin and formin are important actin-interacting proteins, which are involved in flagellum assembly, disassembly, and dynamics (27). However, actin-binding properties of katanin have not been experimentally proved so far. In addition, targeted proteomic analysis of mammalian katanin subunits in HeLa cell lines was used for creation of mammalian katanin family interaction network (Katan-ome), which plays an important role in microtubule severing (28).

Although some developmental and cellular roles of KATANIN 1 in plants were relatively well established, a comprehensive proteome-wide study on *KATANIN 1* mutants was not performed yet. Therefore, the present proteomic dissection of *fra2* and *ktn1-2* mutants provides an important survey of new proteins linked to phenotypic and microtubule defects of these mutants.

EXPERIMENTAL PROCEDURES

Experimental Design and Statistical Rationale—Proteomics analyses were carried out with four biological replicates for each of the six biological samples (roots and aerial parts of Col-0, *fra2,* and *ktn1-2*). Each replicate contained at least 30 seedlings. Pooling of the specimen was necessary to limit the effects of variations between individual plants. The number of replicates was sufficient to ascertain statistical significance, when analysis of variance (ANOVA) was used to test the differences of protein abundances between biological samples. Because a single factor (wild type and mutants represent one factor) was evaluated and the protein abundance datasets exhibit normal (Gaussian) distribution, it was appropriate to apply one-way ANOVA analysis.

Plant Material—Seeds of *ktn1-2, fra2,* and wild type *Arabidopsis thaliana* (ecotype Col-0) were surface-sterilized and placed on half-strength MS culture medium (pH 5.7) containing 1% (w/v) sucrose and 0.8% (w/v) phytagel. Plates with seeds were stored at 4 °C for 48 h to break seed dormancy, and afterward kept vertically in a culture chamber under 16 h light/8 h dark at 22 °C. *fra2* is a single nucleotide mutant in the seventh exon of *KATANIN 1* (At1g80350), where the A at nucleotide residue 2329 is deleted (21). *ktn1-2* is a knockout mutant with T-DNA inserted after the 147th nucleotide in the 5th exon of *KATANIN 1* (16). Fourteen-day-old seedlings were used for proteomic and immunoblotting analyses. For whole-mount immunolabeling, 3-day-old seedlings of *ktn1-2* and *fra2* mutants and Col-0 were used.

Protein Extraction for Proteomic Analysis—Roots and aerial parts of mutant and control plants were subjected to phenol protein extraction, trypsin digestion, and peptide purification as described previously (29).

Fresh material (250 mg) was homogenized in liquid nitrogen with 500 μl of cold extraction medium (0.9 M sucrose, 0.1 M Tris-HCl (pH 8.8), 10 mM EDTA, 100 mM KCl, and 0.4% (v/v) 2-mercaptoethanol) and an equal amount of Tris-HCl-buffered phenol (pH 8.1). The mixture was incubated for 30 min at 4 °C. Then, the protein-enriched phenol phase was separated from the aqueous phase by 5 min of centrifugation at 6000 $\times$ *g* at 4 °C. Phenol phase was subjected to ammonium acetate/methanol precipitation at −20 °C overnight. The precipitate was then pelleted by centrifugation at 13,000 $\times$ *g* at 4 °C for 20 min followed by two washes with ice-cold 80% (v/v) acetone and 1 wash in 70% (v/v) ethanol. Precipitate suspensions were stored at −20 °C for 15 min for each washing step. Finally, the pellets were resuspended in 80% (v/v) acetone, centrifuged, and air-dried for 10 min. Subsequently they were dissolved in 6 M urea in Tris-HCl buffer (pH 7.4). After protein content determination (with Bradford assay), equal amounts of proteins were used for in solution digestion. Prior to trypsin application, protein extracts were subjected to a reduction step (by the addition of 50 mM DTT and incubation for 1 h at room temperature), alkylation step (by addition of 50 mM iodoacetamide and incubation at room temperature for 1 h), and the urea concentration was lowered to less than 1 M. The trypsin digestion (1 μg of sequencing grade modified trypsin from Promega per 50 μg of proteins) was performed by permanent gentle shaking at 37 °C overnight. After stopping trypsin digestion by acetic acid, peptides were cleaned on C18 cartridges (Bond Elut C18; Agilent Technologies, Santa Clara, CA) according to manufacturer's instructions. Peptides eluted by 90% (v/v) acetonitrile were dried using SpeedVac and used for LC-MSMS.

Detailed Description of Liquid Chromatography, Mass Spectrometry, Protein Identification, and Relative Quantitative Analysis—Two μg of protein tryptic digest resuspended in 0.1% (v/v) formic acid, 5% (v/v) acetonitrile were loaded on reversed phase fused silica C18 column measuring 75 μm $\times$ 150 mm (Thermo Fisher Scientific, Waltham, MA). Peptides were separated and eluted at a constant flow rate of 0.3 $\mu l \cdot min^{-1}$ by a 170-min long nonlinear gradient of acetonitrile (in 0.1% formic acid) as follows: 2–55% for 125 min, 95% for 15 min, and 2% for 30 min. The mass spectra were obtained in the data-dependent acquisition mode, with dynamic exclusion being applied, in 18 scan events: one MS scan (*m/z* range, 300–1700) followed by 17 MSMS scans for the 17 most intense ions detected in MS scan. Other critical parameters were set as given here: normalized collision energy, 35%; automatic gain control "on" with MS^n target 4×10^4, isolation width (*m/z*), 1.5; capillary temperature, 170 °C; spray voltage, 1.97 kV. The method and raw spectral files were created and generated, respectively, by Xcalibur 2.1 (Thermo Fisher Scientific).

The raw files were searched using the SEQUEST algorithm of the Proteome Discoverer 1.1.0 software (Thermo Fisher Scientific) with selection of parameters as follows: minimum and maximum precursor mass, 300 and 6,000 Da, respectively; precursor mass tolerance, 1.5 Da; fragment mass tolerance, 0.8 Da; intensity threshold, 1000; minimum ion count, 7; minimum S/N ratio, 3; enzyme, trypsin; maximum missed cleavages, 2; FDR = 0.01; dynamic (variable) modifications,

cysteine carbamidomethylation (+57.021), methionine oxidation (+15.995), and methionine dioxidation (+31.990).

The spectral data were matched against target and decoy databases for more stringent approach to calculating FDR, compared with single search of concatenated database. The NCBI (www.ncbi.nlm.nih.gov) *Arabidopsis* genus taxonomy referenced protein database (67,924 entries as of November, 2013) served as the target database, and its reversed copy (created automatically by the software) served as a decoy database. The search results were filtered by Xcorr values pertinent to +1, +2, and +3 charged peptides, resulting in FDR <1%. Identified proteins were grouped by default parameters of the software, defining the group as proteins strictly necessary to explain the presence of identified peptides. A representative/master protein of the group is the protein with the highest score, spectral count, and number of matched peptides. If those parameters are equal, the protein with the longest sequence is designated as a master protein. Proteins listed in the supplemental materials are master proteins; however, all groups proteins, their accession numbers, respective peptides, and annotated spectra are included in ".msf" files (see below for how to view them). If the peptide can be attributed to more than one protein, it is indicated by multiple protein accession numbers allocated to a given peptide.

The relative quantitative analysis was based on sums of precursor ion intensities (PII) of filtered peptides attributed to given proteins. PII values were extracted from raw files and exported to spread sheets by Proteome Discoverer software. Even though the peptide-respective experimental PII values are not strictly stoichiometric for a given protein, they are commonly accepted for label-free mass spectrometry-based relative protein quantification. Intensities were summed for each identified master protein in each replicate using in house Xcell script. All data points were considered, and no outliers were excluded. Summed intensities pertinent to proteins in individual replicates were normalized by factors that were calculated to equalize total intensity of all master proteins across all biological samples and replicates. Normalized average protein intensities were used to calculate fold changes when comparing biological samples. The ANOVA analysis of four replicates for each biological sample was performed, and $p \leq 0.05$ was used to filter statistically significant results.

Bioinformatic Evaluation of Proteomic Data—Venn diagram was created using Venny 2.1 on-line application (http://bioinfogp.cnb.csic.es/tools/venny/index.html). Differentially abundant proteins were annotated using Gene Ontology annotation analysis by Blast2Go software (30). Blast was performed against *Arabidopsis thaliana* NCBI database allowing 1 BLAST Hit. The annotation was performed by using these parameters: E value hit filter, $1.0E^{-6}$; annotation cutoff: 55; GO weight: 5, GO Slim. For prediction of protein interaction network analysis, STRING (31) applying minimum required interaction score 0.7 was relevant for high confidence prediction.

Immunoblotting Analysis—Roots and aerial parts of wild type and mutant seedlings were crushed in liquid nitrogen to a fine powder. The powder (200 mg) was resuspended and homogenized with 250 μl of 50 mM HEPES (pH 7.5) containing 75 mM NaCl, 1 mM EGTA, 1 mM $MgCl_2$, 10% (v/v) glycerol, 1 mM DTT, and Complete® EDTA-free protease inhibitor mixture (Roche Applied Science) and incubated for 15 min on ice. After centrifugation at 13,000 × *g* at 4 °C for 15 min, the protein amount was quantitated in supernatants. Extracts were proportionally mixed to give a protein concentration of 1.5 mg of protein/ml with 4-fold concentrated Laemmli buffer (final concentration 62.5 mM Tris-HCl (pH 6.8), 2% (w/v) SDS, 10% (v/v) glycerol, 300 mM 2-mercaptoethanol), heat-denaturated at 95 °C for 5 min, and centrifuged to remove undissolved components. Equal amount of proteins (15 μg) were loaded on 12% TGX Stain-Free™ (Bio-Rad) gels. After electrophoresis, proteins were transferred to nitrocellulose membranes using TransBlot™ Turbo (Bio-Rad) semidry transfer system. To validate the protein transfer, membranes were documented on ChemiDoc documentation system (Bio-Rad), allowing visualization of proteins transferred from TGX Stain-Free™ gels. Afterward, they were blocked overnight in 4% (w/v) BSA, 4% (w/v) low-fat dry milk in Tris-HCl-buffered saline with 0.1% (v/v) Tween 20 (TBST). Membranes were then incubated overnight with anti-TSN1/2 (32) (1:750), anti-actin (1:4000; Sigma-Aldrich, Heidelberg, Germany), anti-α-tubulin (clone YOL1/34; 1:2000; ABD Serotec, Raleigh, NC), or anti-β-tubulin (1:2000; Sigma-Aldrich) antibodies, all prepared in TBST with 1% (w/v) BSA. After repeated washings in TBST, membranes were incubated in HRP-conjugated secondary antibody ($F(ab')_2$ goat anti-rabbit IgG (H+L) secondary antibody, HRP; Thermo Fisher Scientific) diluted to 1:5000 in 1% (w/v) BSA in TBST. The signal was developed after washing by TBST using Clarity™ ECL Western blotting substrate (Bio-Rad) and recorded with ChemiDoc™ documentation system (Bio-Rad). Band densities were quantified using ImageLab software (Bio-Rad). All immunoblot analyses were performed at least in three biological replicates. Student's *t* test was applied to evaluate the statistical significance of differences.

Whole-mount Immunolabeling—Immunolocalization of microtubules, KNOLLE and TSN1/2, in root whole mounts was done as described previously (33) with a small modification: cell wall digestion enzyme mixture contained 1% (w/v) meicelase, 1% (w/v) cellulase, and 1% (w/v) macerozyme R10 (Desert Biologicals) in PBS. Samples were immunolabeled with rabbit anti-TSN1/2 (29), rat anti-α-tubulin (clone YOL1/34; ABD Serotec), or rabbit anti-KNOLLE (34) primary antibodies diluted 1:75, 1:300, and 1:2000, respectively, in 3% (w/v) BSA in PBS at 4 °C overnight. In the case of KNOLLE and tubulin, co-localization a double immunolabeling was performed. Secondary antibodies included Alexa-Fluor 488 goat anti-rat and Alexa-Fluor 546 goat anti-rabbit IgGs (Thermo Fisher Scientific) and were diluted 1:500 in PBS containing 3% (w/v) BSA for 3 h (1.5 h at 37 °C and 1.5 h at room temperature). Where necessary, nuclei were counterstained with DAPI. Microscopic analyses of immunolabeled samples were examined with a Zeiss 710 CLSM platform (Carl Zeiss, Jena, Germany), using excitation lines at 405, 488, and 561 nm from argon, HeNe, diode, and diode-pumped solid-state lasers. Images were processed using ZEN 2010 software, Photoshop 6.0/CS, and Microsoft PowerPoint. Fluorescence intensity was evaluated using ZEN 2010 software (Carl Zeiss). Maximum intensity projections from Z-stack images (15 μm thick) of root epidermal cells were used for measurements. At least five individual root tips were analyzed. Student's *t* test was applied to evaluate the statistical significance of differences. Microtubule orientation and degree of isotropy were evaluated using CytoSpectre software (35).

Visualization of Actin Using Alexa-labeled Phalloidin—Actin visualization was performed according Panteris *et al.* (36) with a small modification: after actin stabilization with 200 μM *m*-maleimidobenzoyl-*N*-hydroxysuccinimide ester (BSE), whole seedlings were fixed in a mixture of 2.5% (w/v) paraformaldehyde, 0.5% glutaraldehyde, 10 μM BSE, and 0.1 μM Alexa-Fluor 568 phalloidin in microtubule stabilizing buffer (MTSB; 25 mM K-PIPES (pH 6.8), 2.5 mM EGTA and 2.5 mM $MgSO_4 \cdot 7H_2O$) for 60 min. After washing in MTSB (three times for 2 min), seedlings were extracted in extraction buffer containing 5% (v/v) DMSO, 1% (v/v) Triton X-100 in MTSB for 15 min. Finally, seedlings were stained with 10% (v/v) Alexa-Fluor 488 phalloidin in MTSB for 60 min in the dark. Microscopic analysis of immunolabeled samples was performed using a Zeiss LSM710. Alexa-Fluor 488 phalloidin was excited at 488 nm, and fluorescence was detected between 499 and 566 nm. Images were processed using ZEN 2010 software, Photoshop 6.0/CS, and Microsoft PowerPoint. Actin filament orientation and degree of isotropy were evaluated using CytoSpectre software (35).

TABLE I

List of proteins with significantly different abundances consistently found in fra2 and ktn1-2 mutants as compared with wild type (Col-0). NA = not applicable

Accession no.	Description	Sample	Normalized intensity average in Col-0 roots	Normalized intensity average in *fra2* roots	Normalized intensity average in *ktn1-2* roots	Fold change		*p* value	
						fra2 vs Col-0	*ktn1-2* vs Col-0	*fra2* vs Col-0	*ktn1-2* vs Col-0
Amino acid metabolism									
gi15233111	Cysteine synthase C1	Roots	52115.82	185447.46	136112.56	3.56	2.61	0.05	0.01
gi15223910	Aspartate semialdehyde dehydrogenase	Roots	55508.12	230059.47	125986.93	4.14	2.27	0.05	0.05
Proteolysis									
gi18402225	Granulin repeat cysteine protease family protein	Roots	75658.44	343248.11	448897.32	4.54	5.93	0.01	0.00
Protein synthesis and translation									
gi18410833	50S ribosomal protein L31	Aerial parts	6417292.09	2295801.19	4254452.45	0.36	0.66	0.007	0.023
gi18399100	40S ribosomal protein S18	Roots	113741.22	227944.46	394848.67	2.00	3.47	0.00	0.00
gi15221798	60S ribosomal protein L6-1	Roots	123564.32	196333.48	383764.34	1.59	3.11	0.00	0.01
gi79324564	40S ribosomal protein S5-1	Roots	219962.29	82575.80	94830.59	0.38	0.43	0.01	0.01
gi79317147	50S ribosomal protein L4	Aerial parts	7808895.67	1985714.83	2279779.83	0.25	0.29	0.005	0.003
gi30692346	Small subunit ribosomal protein S1	Aerial parts	8943813.19	5884181.99	5048811.79	0.66	0.56	0.055	0.005
gi15232603	60S acidic ribosomal protein P0-2	Aerial parts	9543945.84	4587130.63	4871300.09	0.48	0.51	0.001	0.009
Energy, metabolism, and photosynthesis									
gi26557005	ATPase subunit 1	Aerial parts	2793480.24	7217395.44	5089236.13	2.58	1.82	0.007	0.030
gi18412632	ATP synthase γ chain 1	Aerial parts	24872995.56	16236642.88	17444031.98	0.65	0.70	0.022	0.030
gi15230595	phosphoglycerate kinase 1	Aerial parts	99022520.01	73663523.69	28363047.45	0.74	0.29	0.026	0.003
gi79313434	γ-Hydroxybutyrate dehydrogenase	Roots	14385.25	0	0	Unique in Col-0		NA	NA
gi145329204	Triose-phosphate isomerase	Roots	148158.00	366354.23	305748.27	2.47	2.06	0.00	0.00
gi15235029	chlorophyll a-b binding protein CP26	Aerial parts	4581201.95	9236218.52	6837980.22	2.02	1.49	0.05	0.033
gi15228194	Sedoheptulose-1,7-bisphosphatase	Aerial parts	8304146.35	13526281.91	13754753.35	1.63	1.66	0.010	0.045
gi15230358	Adenylosuccinate synthetase	Roots	61378.48	0	0	Unique in Col-0		NA	NA
gi7525041	Ribulose-1,5-bisphosphate carboxylase/oxygenase large subunit	Aerial parts	411927407.76	294914235.63	277266195.81	0.72	0.66	0.019	0.019
gi30684767	ATP-dependent zinc metalloprotease FTSH 2 (VAR2)	Aerial parts	10406900.99	5403906.75	6122905.04	0.52	0.59	0.027	0.052
gi15217918	DNA-damage resistance protein DRT112	Aerial parts	13493270.03	2986221.23	4416446.13	0.22	0.33	0.011	0.007
gi15242465	Soluble inorganic pyrophosphatase 1	aerial parts	11022571.57	5807403.25	5763606.13	0.53	0.52	0.044	0.027
gi238479213	Ribulose bisphosphate carboxylase large chain, catalytic domain	Aerial parts	15069515.17	10777815.24	9451326.29	0.72	0.63	0.021	0.021
Stress response and redox regulation									
gi15236014	Lipase/lipooxygenase, PLAT/LH2 family protein	Roots	38041.31	0	0	Unique in Col-0		NA	NA
gi18413214	Nucleoside diphosphate kinase 1	Roots	226388.99	380425.14	393491.58	1.68	1.74	0.02	0.39
gi15235401	Glutathione *S*-transferase F2	Roots	644121.71	1578139.78	2106336.43	2.45	3.27	0.00	0.01
gi15230982	Peroxiredoxin Q	Aerial parts	9363992.23	5543512.31	3980676.95	0.59	0.43	0.042	0.005
gi79313261	PYK10-binding protein 1	Roots	1166764.61	630062.78	644475.44	0.54	0.55	0.01	0.01
gi18415805	Ferredoxin/thioredoxin reductase subunit A (variable subunit) 2	Aerial parts	2441812.37	895399.11	1305568.55	0.37	0.53	0.011	0.053
gi15236386	Selenium-binding protein 2	Aerial parts	1289730.38	0	0	Unique in Col-0		NA	NA
gi15234648	Peroxidase 45	Roots	447213.47	690524.52	951861.94	1.54	2.13	0.05	0.02
Signaling									
gi18413181	14-3-3-like protein GF14 chi	Roots	797937.21	0	0	Unique in Col-0		NA	NA
Hormonal homeostasis									
gi42570831	*S*-Alkyl-thiohydroximate lyase SUR1	Roots	6362.74	0	0	Unique in Col-0		NA	NA
gi15221692	Pyruvate dehydrogenase E1 component subunit α-2 (IAR4)	Roots	253127.82	55389.52	66337.07	0.22	0.26	0.01	0.02
Protein folding, chaperones									
gi334185828	Clp ATPase	Roots	107823.61	37454.35	48712.02	0.35	0.45	0.02	0.03
gi18415982	Tetratricopeptide repeat protein	Roots	222702.14	427357.63	486498.43	1.92	2.18	0.03	0.02
gi15237739	Cyclophilin ROC7	Aerial parts	10957142.37	3657898.57	3546535.06	0.33	0.32	0.002	0.004

TABLE I—*continued*

Accession no.	Description	Sample	Normalized intensity average in Col-0 roots	Normalized intensity average in *fra2* roots	Normalized intensity average in *ktn1-2* roots	Fold change		*p* value	
						fra2 vs Col-0	*ktn1-2* vs Col-0	*fra2* vs Col-0	*ktn1-2* vs Col-0
Unknown function									
gi18404496	NAD(P)-binding Rossmann-fold-containing protein	Aerial parts	8607872.32	5447058.47	5603099.42	0.63	0.65	0.008	0.007
gi15237739gi15224648	Membrane-associated progesterone binding protein 2	Roots	203330.29	371469.14	439583.49	1.83	2.16	0.03	0.02
gi15237739gi30682601	Vacuolar calcium-binding protein-like protein	Roots	57633.53	242968.33	103128.61	4.22	1.79	0.01	0.05
gi15237739gi334187997	Uncharacterized protein	Aerial parts	739698.22	0	0	Unique in Col-0		NA	NA
Membrane transport									
gi15237739gi18397991	MD-2-related lipid recognition domain-containing protein	Roots	102011.46	0	0	Unique in Col-0		NA	NA

Quantitative Analysis of mRNA Transcript Levels by Real-time PCR—Total RNA was extracted from roots and aerial parts of 14-day-old seedlings of Col-0, *fra2,* and *ktn1-2* mutants using TRI Reagent® (Sigma-Aldrich) according to the manufacturer's protocol. After DNase I digestion, RNA concentration and purity were determined with NanoDrop Lite spectrophotometer (Thermo Fisher Scientific). Template-primer mix for reverse transcription was composed of 1 μl of oligo(dT) primers (0.5 μg per reaction), 1.5 μg of RNA, and PCR-grade distilled water in total volume of 20 μl. The mixture was denatured at 65 °C for 5 min. The following components were added: 4 μl M-MLV reverse transcriptase 5$\times$ reaction buffer (Promega), 2 μl of deoxynucleotide mix (10 mM), 1 μl (40 units) RNasin® Plus RNase inhibitor (Promega), 1 μl (100 units) of M-MLV reverse transcriptase (Promega), and PCR-grade distilled water, in a total volume of 20 μl. PCRs were performed at 42 °C for 1 h followed by inactivation at 70 °C for 10 min. After reverse transcription reaction, the mixture was diluted four times. Quantitative RT-PCRs were performed in a 96-well plate with StepOnePlus Real-time PCR system (Applied Biosystems, Foster City, CA) using SYBR® Green to monitor dsDNA synthesis. Reaction contained 5 μl of Power SYBR® Green PCR master mix (Thermo Fisher Scientific), 0.75 μl of cDNA (corresponds to 140 ng of RNA before reverse transcription), and 0.5 μM gene-specific primers (supplemental Table S1). The following standard thermal profile was used for all PCRs: 95 °C for 10 min, 40 cycles of 95 °C for 15 s, and 60 °C for 1 min. Experiments were run in three biological replicates, and the intra-assay variability was determined with technical triplicates. The expression data were normalized to the expression of *EF1*α (*ELONGATION FACTOR 1-*α; At5g60390) as a reference gene, and relative gene expression was calculated by $2^{-\Delta\Delta Cq}$ method. Specificity of the target amplification was further verified by melting curve analysis of reaction products.

RESULTS

Overview of Proteomic Analysis and Functional Classification of the Differential Proteome—In addition to complete mass spectrometry/proteomics data deposited to PRIDE (see above), the information pertinent to protein identification can be found in the supplemental material in the form of common Excel files given for each individual sample. We compared the proteomes of roots and aerial parts of *fra2* and *ktn1-2* mutants with Col-0 quantitatively. Only those proteins that differed in abundance more than 1.5-fold between wild type and both mutants have been considered. Forty two proteins, 22 in roots and 20 in aerial parts, were differentially abundant in both mutants and showed a consistent trend in abundance difference (Table I). Twenty six of them were down-regulated, and 16 were up-regulated. Quantification details of all proteins identified in the mutants are presented in supplemental Table S2 (roots) and supplemental Table S3 (aerial parts). We have detected 69 and 45 differentially abundant proteins in roots of *fra2* and *ktn1-2*, respectively. In aerial parts, 53 and 51 differentially regulated proteins were identified in *fra2* and *ktn1-2* (Fig. 1, *A* and *B*). Among them, seven proteins in roots and two proteins in aerial parts were identified only in Col-0, but they were not identified in the mutants. It is likely that differences in proteomes of these two mutants might arise from distinct types of mutations (mentioned under "Experimental Procedures").

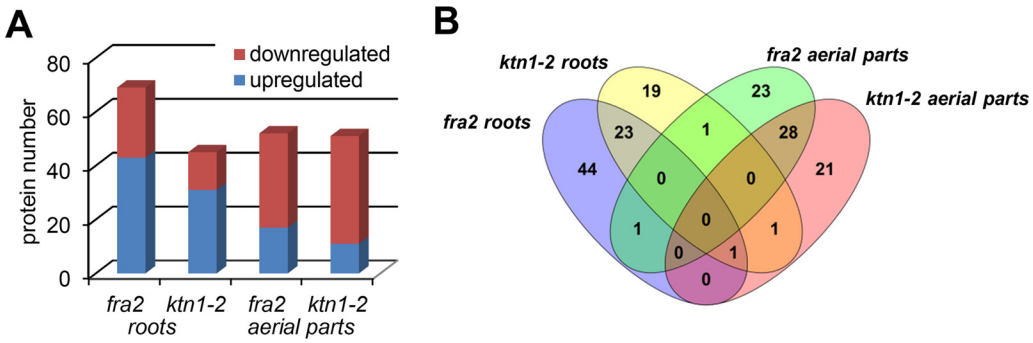

FIG. 1. **Outputs of proteomic analysis of *KATANIN 1* mutants.** *A, graph* showing numbers of proteins with increased or decreased abundances in roots and aerial parts of *fra2* and *ktn1-2* mutants as compared with the Col-0 wild type. *B,* Venn diagram showing numerical distribution of proteins with significantly changed abundances among roots and aerial parts of *fra2* and *ktn1-2* mutants.

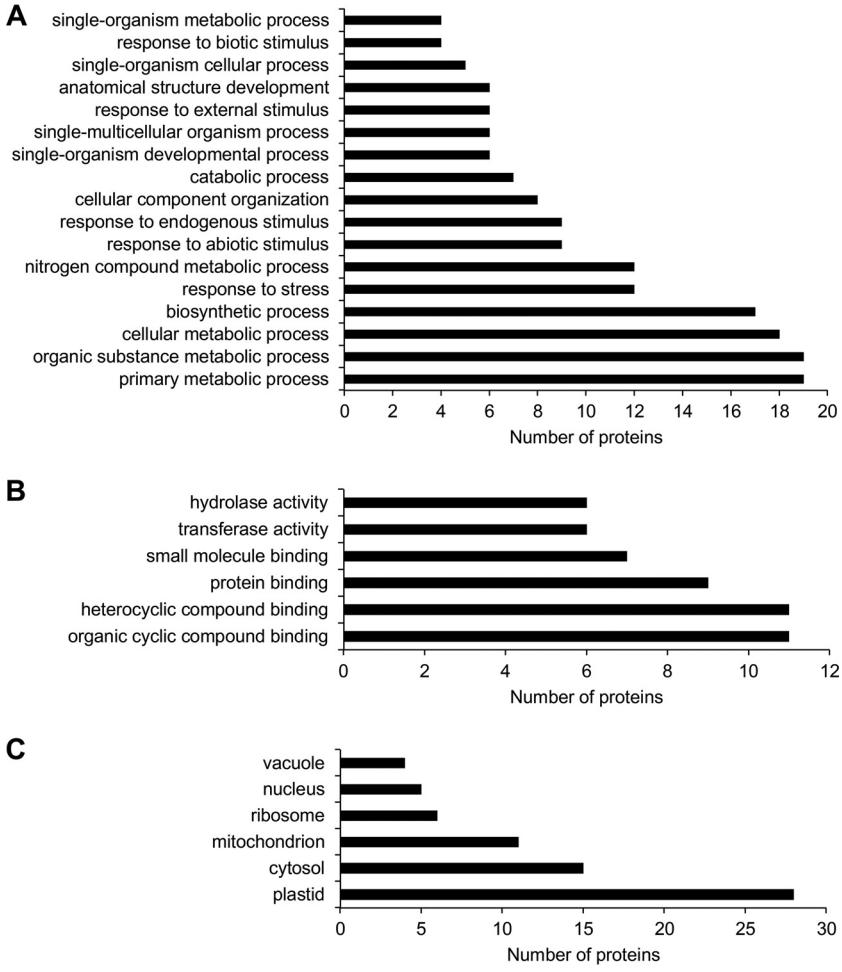

FIG. 2. ***Graphs* showing GO annotations of differentially abundant proteins found consistently in *fra2* and *ktn1-2* mutants (roots and aerial plants collectively) according to biological process (*A*), molecular function (*B*), and cellular compartments (*C*).**

We used gene ontology (GO) annotation to evaluate the impact of defective microtubule severing on the *Arabidopsis* proteome. According to biological process, the highest number of differentially abundant proteins was annotated to diverse metabolic processes (Fig. 2*A*). A significant number of proteins was also denoted as involved in the response to biotic and abiotic stimuli. Last but not least, GO annotations connected to cellular component organization and development showed changed abundances in both mutants (Fig. 2*A*). According to molecular functions, differentially abundant proteins were involved in binding to proteins, organic and inorganic compounds, as well as binding to small molecules (Fig. 2*B*). GO annotation according to cell compartment showed different abundances of proteins localized to plastids, cytosol, mitochondria, ribosomes, nuclei, and vacuoles (Fig. 2*C*). A detailed GO annotation performed separately for differentially

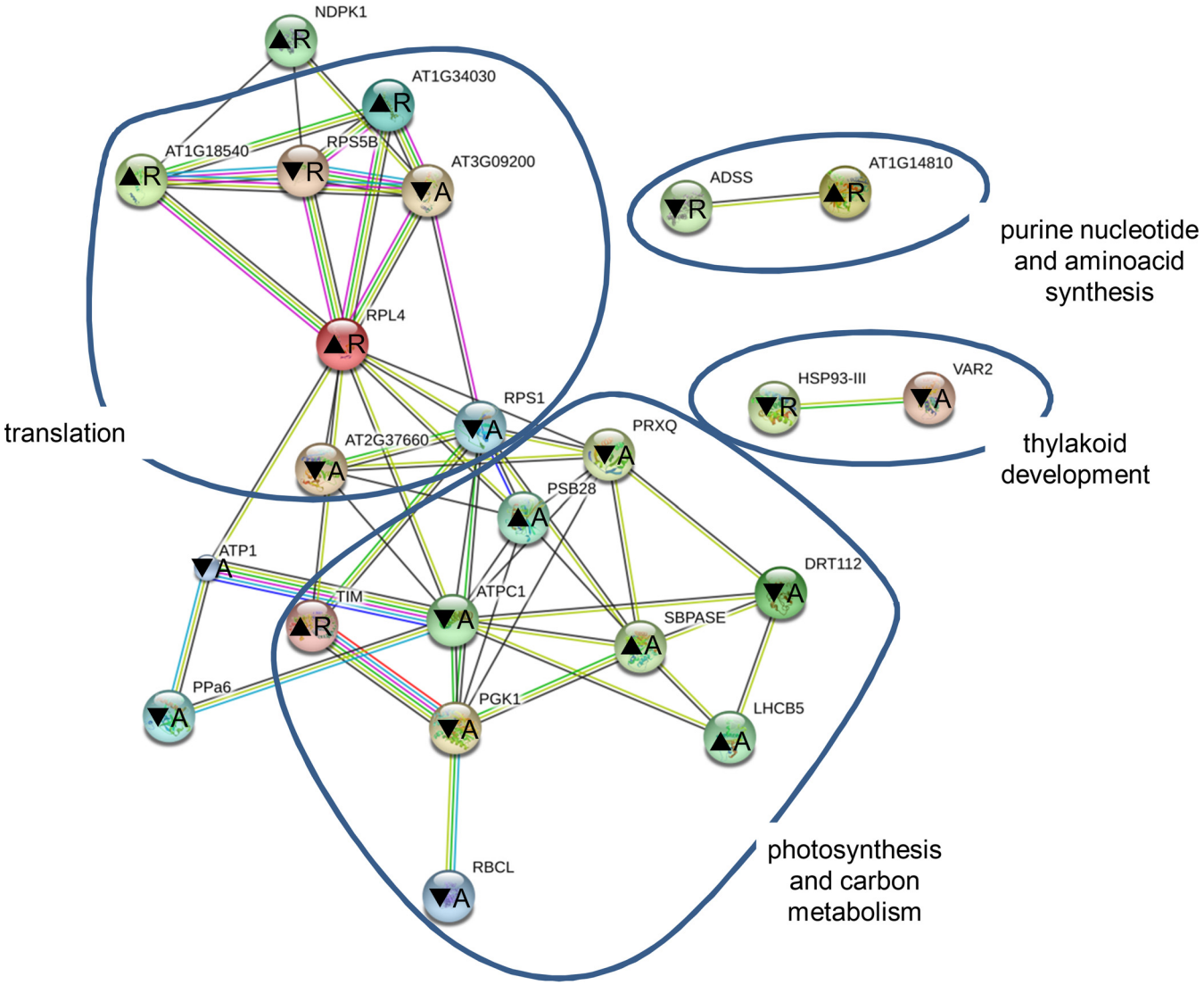

FIG. 3. **Representation of protein interaction networks in differential proteome consistently found in both *fra2* and *ktn1-2* roots and aerial parts and as generated by STRING web-based application.** *Letters* in nodes mean roots (*R*) and aerial (*A*) parts. ▲ means increased abundance, and ▼ means decreased abundance. Different *line colors* represent the types of evidence used in predicting the associations: gene fusion (*red*), neighborhood (*green*), co-occurrence across genomes (*blue*), co-expression (*black*), experimental (*purple*), association in curated databases (*light blue*), or co-mentioned in PubMed abstracts (*yellow*). RPL4 is 50S ribosomal protein L4 (gi79317147); At1g14810 is aspartate semialdehyde dehydrogenase (gi15223910); ADSS is adenylosuccinate synthetase (gi15230358); At1g18540 is 60S ribosomal protein L6-1 (gi15221798); DRT112 is DNA-damage resistance protein DRT112 (gi15217918); At1g34030 is 40S ribosomal protein S18 (gi18399100); TIM is triose-phosphate isomerase (gi145329204); VAR2 is ATP-dependent zinc metalloprotease FTSH 2 (VAR2) (gi30684767); RPS5B is 40S ribosomal protein S5-1 (gi79324564); At2g37660 is NAD(P)-binding Rossmann fold-containing protein (gi18404496); At3g09200 is 60S acidic ribosomal protein P0-2 (gi15232603); PGK1 is phosphoglycerate kinase 1 (gi15230595); PRXQ is peroxiredoxin Q (gi15230982); HSP93-III is Clp ATPase (gi334185828); SBPASE is sedoheptulose-1,7-bisphosphatase (gi15228194); ATPC1 is ATP synthase γ chain 1 (gi18412632); NDPK1 is nucleoside diphosphate kinase 1 (gi18413214); LHCB5 is chlorophyll *a-b*-binding protein CP26 (gi15235029); PSB28 is photosystem II reaction center PSB28 protein (gi18417239); PPa6 is soluble inorganic pyrophosphatase 1 (gi15242465); RPS1 is small subunit ribosomal protein S1 (gi30692346); RBCL is ribulose-1,5-bisphosphate carboxylase/oxygenase large subunit (gi7525041); and ATP1 is ATPase subunit 1 (gi26557005).

regulated proteins in roots and aerial parts is provided in supplemental Figs. S1–S6.

Analysis of protein interaction networks occurring among these proteins using STRING application showed deregulation of proteins involved in photosynthesis, carbon metabolism, and translation in both mutants (Fig. 3). Other less abundant networks were annotated to purine nucleotide and amino acid synthesis and chloroplast thylakoid development. The majority of proteins involved in photosynthesis showed decreased abundance in the mutants, whereas carbon metabolism appears to be enhanced. Two proteins contributing to thylakoid development showed unequivocal decreased abun-

TABLE II

Differentially abundant proteins having developmental roles in fra2 and ktn1-2 mutants

Proteins annotated in GO cellular component organization (GO:0016043), single organism developmental process (GO:0044767), anatomical structure development (GO:0048856), and proteins reported to have developmental roles are listed.

Accession no.	Description	Sample	Fold change		GO annotation	Experimental evidence
			fra2 vs Col-0	*ktn1-2* vs Col-0		
gi15221692	Pyruvate dehydrogenase E1 component subunit α-2 (IAR4)	Roots	0.22	0.26		Auxin homeostasis (67, 68)
gi42570831	*S*-Alkyl-thiohydroximate lyase SUR1	Roots	Unique in Col-0		GO:0016043 GO:0044767 GO:0048856	Auxin homeostasis (66)
gi18397991	MD-2-related lipid recognition domain-containing protein	Roots	Unique in Col-0			Gravitropism, auxin transport (72)
gi18413181	14-3-3-like protein GF14 χ	Roots	Unique in Col-0			Regulation of ethylene synthesis (62)
gi18402225	Granulin repeat cysteine protease family protein	Roots	4.54	5.93		ABA signaling (73)
gi334185828	Clp ATPase	Roots	0.35	0.45	GO:0016043	Photosystem biogenesis, thylakoid membrane biogenesis, leaf development (74)
gi79324564	40S ribosomal protein S5-1	Roots	0.38	0.43	GO:0016043	Delayed embryo development, abnormal venation (75)
gi79317147	50S ribosomal protein L4	Aerial parts	0.25	0.29		Embryo development (76)
gi22326646	TUDOR-SN protein 1	Roots	1.50			Embryogenesis and fertility (78)
gi15240352	TUDOR-SN protein 2	Roots	4.48	3.12		Embryogenesis and fertility (78)
gi15237739	Cyclophilin ROC7	Aerial parts	0.33	0.32	GO:0044767 GO:0048856	
gi30684767	ATP-dependent zinc metalloprotease FTSH 2 (VAR2)	Aerial parts	0.52	0.59	GO:0016043 GO:0044767 GO:0048856	Photosystem biogenesis, thylakoid membrane biogenesis, leaf development (74)
gi334187997	Uncharacterized protein	Aerial parts	Unique in Col-0		GO:0016043	
gi15236386	Selenium-binding protein 2	Aerial parts	Unique in Col-0		GO:0016043 GO:0044767 GO:0048856	
gi145329204	Triose-phosphate isomerase	Roots	2.47	2.06	GO:0016043 GO:0044767 GO:0048856	
gi15233111	cysteine synthase C1	Roots	3.56	2.61	GO:0044767 GO:0048856	
gi15235029	Chlorophyll *a*-*b*-binding protein CP26	Aerial parts	2.02	1.49	GO:0016043	
gi79325183	Plasma membrane-associated cation-binding protein 1 (MDP25)	Roots	1.61			Hypocotyl elongation (37, 38)
gi15241472	Tubulin β-4 chain	Roots	0.20			Cell division and elongation (5), seed imbibition (41, 77)
gi18401618	WPP domain-containing protein 2	Roots	0.46			Root growth, cell division (39)
gi15224838	Profilin 1	Roots	1.09	1.48		Cell elongation (79), embryo development and germination (80)
gi30697298	Actin-depolymerizing factor 3	Aerial parts		0.30		Tip growth (81)
gi15242516	Actin 7	Aerial parts	2.09			Root growth (82), seed imbibition (41, 83)
gi15222929	V-type proton ATPase subunit B1	Aerial parts	1.23			Actin stabilizing (84)
gi15219901	Patellin 2	Roots		0.22		Cell plate formation (54)
gi18391066	2,3-Bisphosphoglycerate-independent phosphoglycerate mutase 1	Roots	1.78			Stomatal movements, pollen development (85)

dance. Abundances of proteins involved in translation did not show uniform changes in the mutants. Similar protein networks were predicted when both mutants were analyzed separately (supplemental Fig. S7).

KATANIN1 Mutants Exert Altered Abundances of MAPs, Disturbed Microtubule Organization, and Abnormal Nuclear Shape—Disrupted microtubule severing resulted in severe developmental defects of *fra2* and *ktn1-2* mutants (21, 23, 26). Several proteins related to microtubule severing may contribute to these developmental phenotypes. Therefore, by performing differential proteomics on *fra2* and *ktn1-2* mutants, we focused on proteins involved in plant development as classified by gene ontology annotation (supplemental Tables S4–S7) or experimentally (Table II). These proteins are mostly involved in embryogenesis, germination, root growth, and hypocotyl elongation.

Our proteomic analysis revealed several cytoskeletal and cytoskeleton-related proteins. Interestingly, these proteins form a functionally interconnected network consisting of both microtubule-binding as well as actin-binding and regulatory proteins, as predicted by STRING (Fig. 4). Among them, tubulin β-4 was down-regulated in aerial parts of *fra2* (Table II). To validate such down-regulation, we carried out an immunoblotting analysis of *fra2* and *ktn1-2* roots using anti-β-tubulin antibody. In agreement with proteomic data, β-tubulin showed decreased abundances in both mutants (Fig. 5, *A–C*). As expected, a similar trend was observed in the case of α-tubulin (Fig. 5, *D–F*). Whole-mount immunofluorescence la-

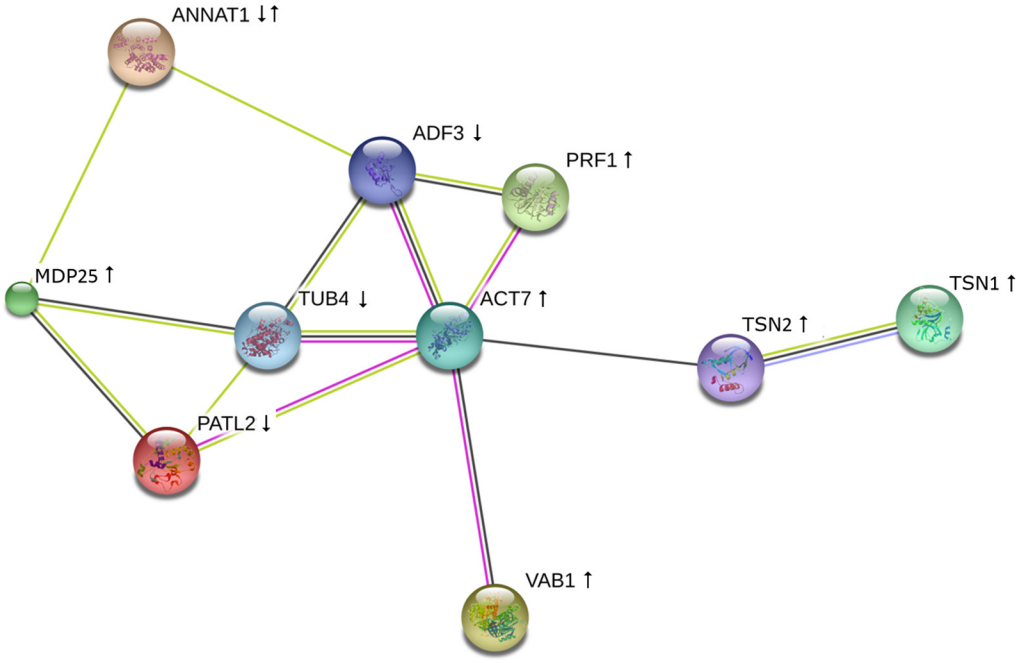

FIG. 4. **Depiction of functional protein association networks predicted by STRING among cytoskeletal proteins found to be differentially abundant in *fra2* and *ktn1-2* as compared with Col-0.** Different *line colors* represent types of evidence used in predicting associations: gene fusion (*red*); neighborhood (*green*); co-occurrence across genomes (*blue*); co-expression (*black*); experimental (*purple*); association in curated databases (*light blue*); or co-mentioned in PubMed abstracts (*yellow*). ↑ means increased abundance; ↓ means decreased abundance. TUB4 is tubulin β-4 chain; TSN1 is TUDOR-staphylococcal nuclease protein 1, TSN2; MDP25 is microtubule-destabilizing protein 25; PATL2 is patellin 2; PRF1 is profilin 1; ACT7 is actin 7; ADF3 is actin-depolymerizing factor 3; ANNAT1 is annexin 1; and VAB1 is V-type proton ATPase subunit B1.

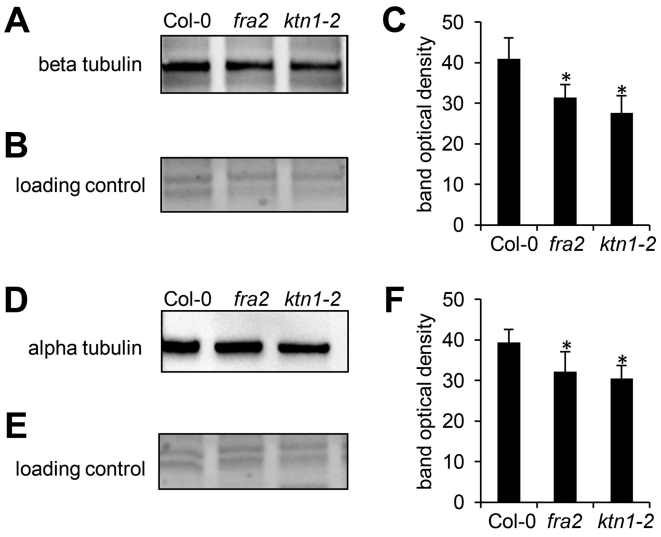

FIG. 5. **Immunoblotting analysis of β-tubulin and α-tubulin in roots of *Arabidopsis* wild type Col-0 and *KATANIN 1* mutants *fra2* and *ktn1-2*.** *A* and *D,* immunoblots probed with anti-β-tubulin (*A*) and anti-α-tubulin (*D*) antibodies. *B* and *E,* visualization of proteins transferred on nitrocellulose membranes. *C* and *F,* optical density quantifications of respective bands in *A* and *D*. *Asterisks* indicate significant differences between mutants and wild type at $p \leq 0.05$ according to Student's *t* test. *Error bars* represent standard deviations.

beling of microtubules performed on root cells revealed reorganization and randomization of microtubules in root epidermal cells of *fra2* and *ktn1-2* mutants (Fig. 6). Furthermore, plasma membrane-associated cation-binding protein 1, also called microtubule-depolymerizing protein 25 (MDP25) (37, 38), showed an increased abundance in the *fra2* mutant (Table II). In addition, we have found proteins controlling microtubule-dependent processes such as cell division and cell plate formation (patellin 2 and WPP domain-containing protein 2; Table II). This is in agreement with the obliquely oriented cell plates in *fra2* and *lue1* mutants as it was previously proposed due to the aberrantly oriented phragmoplasts (24). Our more detailed whole-mount immunolabeling of cell plates using specific antibody recognizing cell plate marker protein KNOLLE (34) showed obliquely oriented and misaligned cell plates in the *ktn1-2* mutant (supplemental Fig. S8), and misaligned phragmoplasts were observed by simultaneous co-visualization of microtubules by using anti-α-tubulin antibody (supplemental Fig. S8). It seems that patellin 2 and WPP2 are co-regulated with KATANIN 1 to control phragmoplast and cell plate formation.

Because WPP2 is also a nuclear envelope localized protein (39), its down-regulation might indicate altered nuclear shape in *KATANIN 1* mutants. Consistent with this assumption, vi-

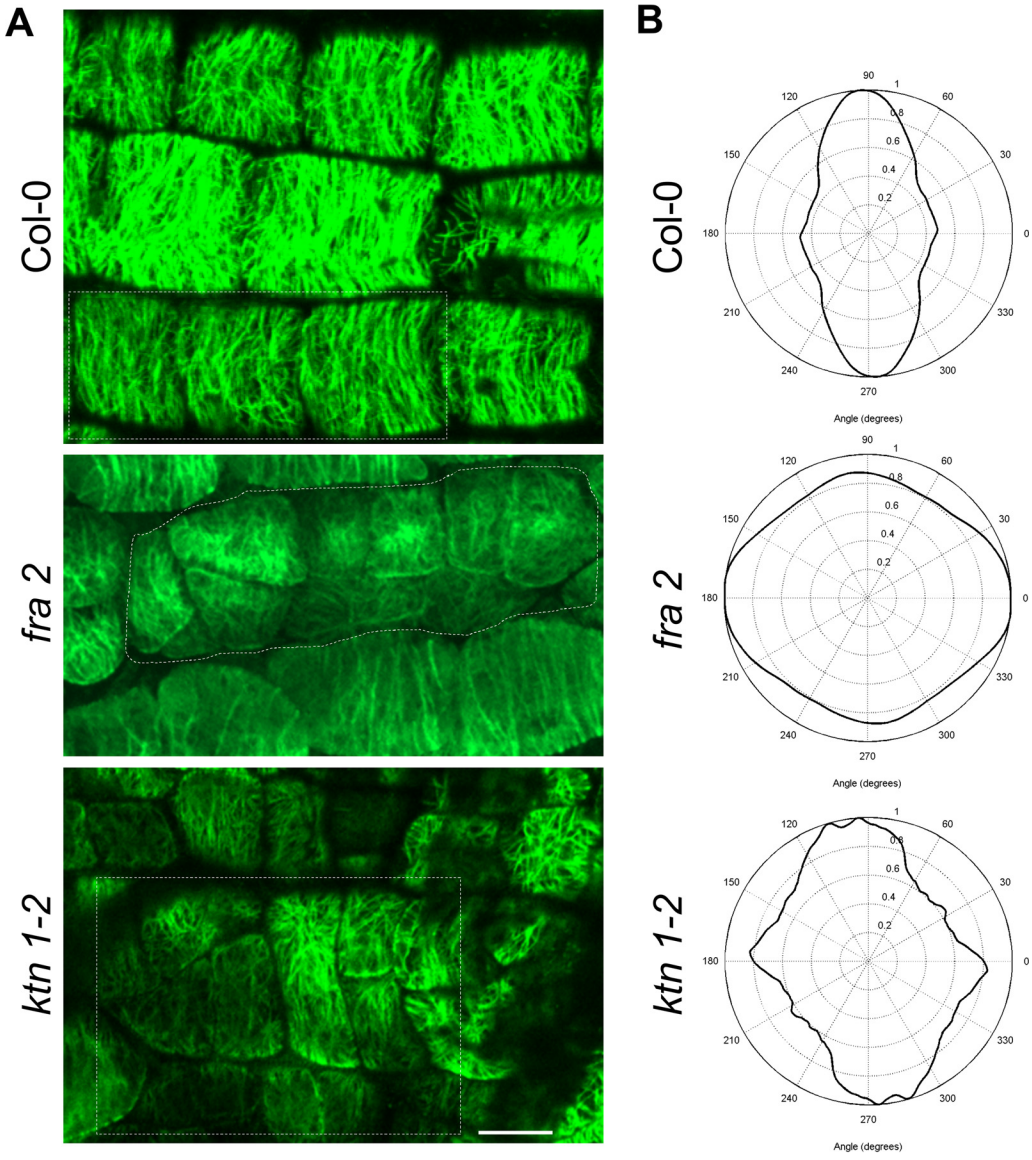

FIG. 6. *A,* immunolocalization of cortical microtubules in root epidermal cells of *Arabidopsis* wild type Col-0 and *KATANIN 1* mutants *fra2* and *ktn1-2*. *B,* microtubule orientation and degree of isotropy analyzed by CytoSpectre software. Note distorted microtubule orientation and anisotropy in both mutants in contrast to mostly parallel microtubule orientation in Col-0. *Bar,* 10 μm.

sualization of nuclei by DAPI revealed that nuclei of *fra2* and *ktn1-2* root epidermal cells showed aberrant shapes (supplemental Fig. S9).

We have also detected increased abundances of TUDOR-staphylococcal nuclease protein 1 (TSN1) and TSN2 in the *fra2* mutant (Table II). These proteins are co-localizing with and move along cortical microtubules (32). They are involved in the formation of stress granules, which is dependent on microtubule dynamics (32). Thus, our results support a tight link between TSN proteins and microtubules. Immunoblotting analysis using primary antibody recognizing both TSN1 and TSN2 verified increased abundances of these two isoforms in *fra2* and *ktn1-2* roots (Fig. 7). This was further confirmed by immunolocalization of TSN proteins in intact roots of *fra2* and *ktn1-2* mutants (Fig. 8). Root cells of both mutants showed prominent accumulation of TSN proteins preferentially at cell peripheries and in the whole cytoplasm that was not so prominent and was quantitatively less abundant in the control Col-0. Altogether, these data indicate a feedback mechanism controlling microtubule organization in *KATANIN 1* mutants.

Defective Microtubule Severing Altered Actin Regulatory Proteins and Actin Organization—Notably, defective microtubule severing in the mutants affected abundances of actin and actin-binding proteins (ABPs). Thus we have found up-regulation of profilin 1 in roots of the *ktn1-2* mutant and up-regulation of actin 7 in *fra2* aerial parts (Table II). The abundance of actin-binding vacuole-type proton ATPase subunit B1 was also increased in aerial parts of *fra2* (Table II). Verifi-

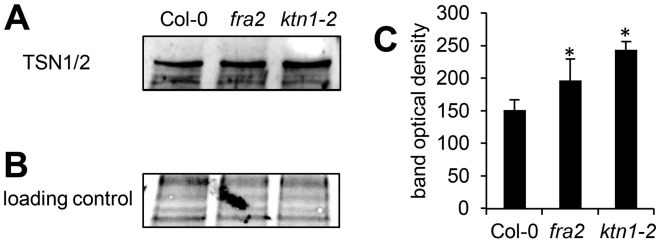

FIG. 7. **Immunoblotting analysis of TSN1/2 (TUDOR-staphylococcal nuclease protein 1/2) abundances in roots of *Arabidopsis* wild type Col-0 and *KATANIN 1* mutants *fra2* and *ktn1-2*.** *A,* immunoblots probed with anti-TSN1/2 antibody. *B,* visualization of proteins transferred on nitrocellulose membranes. *C,* optical density quantification of band in *A*. *Asterisks* indicate significant differences between mutants and wild type at $p \leq 0.05$ according to the Student's *t* test. *Error bars* represent standard deviations.

cation of actin abundances in the mutants and Col-0 control using immunoblotting with an antibody recognizing denatured monomeric G-actin approved the proteomic data (Fig. 9). In addition, actin-depolymerizing factor 3 was negatively regulated in the *ktn1-2* aerial parts (Table II). Importantly, visualization of F-actin by staining with fluorescently labeled phalloidin showed that proteomic changes of actin 7 isoform (up-regulation) and actin-depolymerizing factor 3 (ADF3, down-regulation) led to reorientation and disorganization of actin filaments in leaves of *fra2* and *ktn1-2* mutants. Thus, actin filaments in the leaf epidermal cells of both mutants were more distorted, less abundant, and also less bundled in these cells (Fig. 10). These results suggested a tight cross-talk between microtubules and organization of the actin cytoskeleton in *KATANIN 1* mutants.

Abundances of Cytoskeletal Proteins and Transcript Levels of Corresponding Genes Are Not Correlated in the KATANIN1 Mutants—*KATANIN 1* mutants exhibit severe developmental defects that may cause general transcriptional reprogramming. This may imply that the changes of cytoskeletal proteins in *KATANIN 1* mutants resulted from altered transcriptional regulation and not from direct effects of impaired microtubule-severing activity. Therefore, we quantitatively examined expression levels of genes encoding the most-important 11 cytoskeletal and cytoskeleton-related proteins found by proteomic analysis. In all cases, except *TUBULIN β-4* (*TUB4*) in *fra2,* we have found only minor insignificant changes in the mRNA levels of both *KATANIN 1* mutants as compared with the control (Fig. 11). This indicates that changes in protein abundances were not caused by transcriptional alterations in the mutants.

Proteins Involved in Hormonal Homeostasis Showed Altered Abundances in KATANIN 1 Mutants—Generally, it is known that microtubule cytoskeleton is sensitive to hormones (40), whereas abundance of TUBULIN α2 (TUA2) is controlled by gibberellic acid in *Arabidopsis* (41). In addition, KATANIN 1 participates in the regulation of microtubule reorganization induced by gibberellic acid and ethylene (26). Interestingly, we have found several proteins involved in the regulation of auxin, ethylene (Table II), and gibberellic acid (Tables III and IV) homeostasis. Moreover, a screening of abscisic acid-responsive elements in the promoter sequences of genes encoding identified differentially regulated proteins indicated that proteins involved in ABA response might be also affected by impaired microtubule severing (Table V). Thus, our study also provides new protein candidates for the cross-talk between hormones and microtubules.

DISCUSSION

Although proteomics are effective in identification of proteins regulating cytoskeletal organization, it has been only rarely exploited for this aim in current plant-oriented research. Targeted proteomic approaches were used to identify microtubule-binding proteins (42), whereas proteomic analysis of detergent-resistant and -sensitive membranous fractions combined with cytoskeletal inhibitor treatments revealed the cytoskeleton-dependent distribution of plasma membrane proteins (43). Recently, changes in the abundance of proteins involved in the vesicular transport, RNA nuclear export, and ABA response were reported in response to the actin-depolymerizing drug latrunculin B (44). In mammalian cells, where microtubule severing is more complex as in plants, a proteomic approach was adopted to define the protein interaction module consisting of katanin, katanin-like protein isoforms, and various microtubule-associated proteins (28). However in plants, neither altered cytoskeletal protein profiles nor cross-talk to the actin cytoskeleton was reported in the mutants defective in microtubule-associated protein so far. This study combining genetic (mutants), proteomic, biochemical, and cell biological approaches provides new evidence that defects in microtubule severing by KATANIN 1 caused significant changes in abundances of tubulins, MAP, actin, and ABPs concomitant to global reorganization of microtubules and actin cytoskeleton. In this way, this study revealed a feedback mechanism in the regulation of microtubule organization and uncovered a novel cross-talk mechanism between microtubule and actin cytoskeleton in *Arabidopsis*.

Defective Microtubules and Actin Cytoskeleton in KATANIN 1 Mutants—It is generally accepted that defective microtubule severing impairs cell elongation and promotes isotropic growth leading to profound phenotypic manifestations in *KATANIN 1* mutants (20, 21, 26). KATANIN 1 is activated by Rho GTPase ROP6 via binding to the activator RIC1 (19). Microtubule severing by KATANIN 1 is also regulated by the microtubule-associated protein SPIRAL2 defining where the severing occurs (18). Our proteomic analysis revealed that roots of *fra2* mutant exerted a decreased abundance of TUB4 and increased abundance of TSN1, TSN2, as well as microtubule-destabilizing protein MDP25.

TSN proteins are components of cytoplasmic messenger ribonucleoprotein (mRNP) complexes called stress granules. Such stress granules are sites of post-transcriptional gene

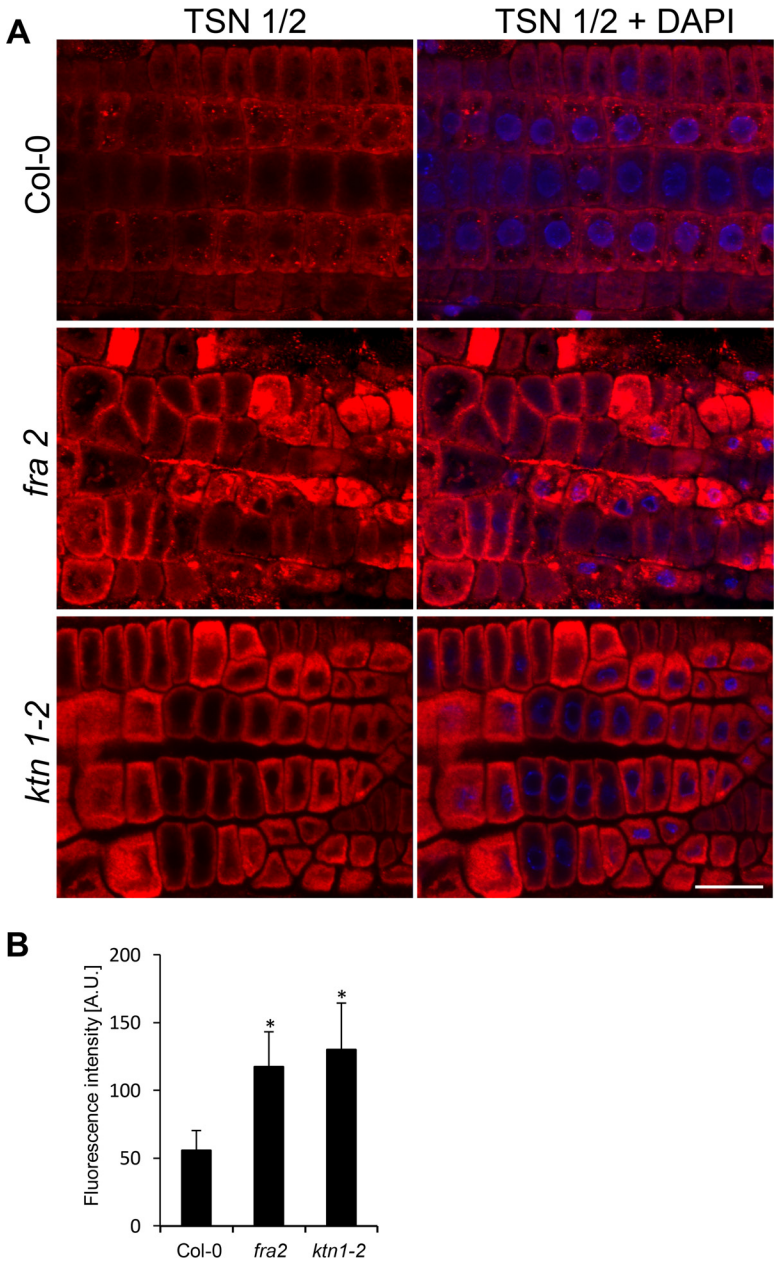

FIG. 8. *A,* immunolocalization of TSN1/2 (TUDOR-staphylococcal nuclease protein 1/2) in root epidermal cells of *Arabidopsis* wild type Col-0 and *KATANIN 1* mutants *fra2* and *ktn1-2*. *B,* fluorescence intensity quantification of immunolabeled TSN1/2 in root epidermal cells of wild type Col-0 and *fra2* and *ktn1-2* mutants. Maximum intensity projections from z-stack images (15 μm thick) of root epidermal cells were used for measurements. At least five individual root tips were analyzed. Differences between both mutants and Col-0 were statistically significant ($p \leq 0.05$) according to Student's *t* test. *Bar,* 20 μm.

silencing, and TSN proteins are important for stress-induced mRNA decapping thus modulating the abiotic stress responses. Importantly, stress granules assemble under stress conditions in a KATANIN 1-dependent manner, and TSN proteins co-localize and move along cortical microtubules (32). This might suggest their potential role in the regulation of microtubule organization. Our data indicate that abundances and subcellular accumulation of TSN proteins are dependent on microtubule severing. MDP25 is a plasma membrane-associated protein, which dissociates from the membrane in a calcium-dependent manner exerting inhibition of microtubule polymerization (37). Interestingly, MDP25 overexpression leads to reduced cell elongation and cortical microtubule reorientation (37), similarly to *KATANIN 1* mutants. Along with reorganization of microtubules in both *KATANIN 1* mutants, it suggests a feedback microtubule control and possible link between MDP25 and microtubule severing in *Arabidopsis*. Moreover, MDP25 is also capable of calcium-dependent binding to F-actin and its severing (38). Another link to the actin cytoskeleton is provided by co-expression of *TSN2* with *ACTIN7* (Fig. 4). Our proteomic analysis revealed alterations in actin and important ABPs (PRF1 and ADF3) in *KATANIN 1* mutants, very likely contributing to disturbances in the actin organization. This was consistent with reoriented and distorted actin filaments, which we observed in leaf epidermal cells of *fra2* and *ktn1-2* mutants. Moreover, we found up-regulation of annexin 1 in aerial parts of both mutants. Interestingly, phosphorylation of annexin A2 (closely related to

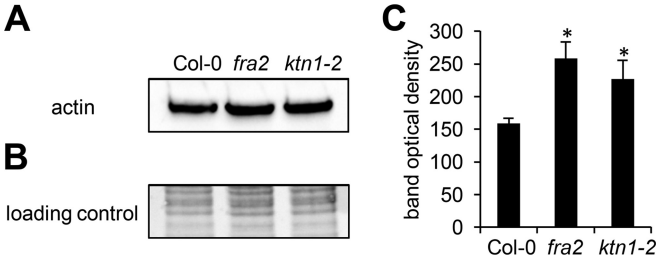

FIG. 9. **Immunoblotting analysis of actin in aerial parts of *Arabidopsis* wild type Col-0 and *KATANIN 1* mutants *fra2* and *ktn1-2*.** *A,* immunoblots probed with anti-actin antibody recognizing both monomeric G-actin and filamentous F-actin. *B,* visualization of transferred proteins on nitrocellulose membranes. *C,* optical density quantification of bands in *A*. *Asterisks* indicate significant differences between mutants and wild type at $p \leq 0.05$ according to the Student's *t* test. *Error bars* represent standard deviations.

annexin 1) was found to be essential for actin cytoskeleton dynamics (45). Cross-talk between microtubule and the actin cytoskeleton was widely documented (46–48). Quantitative live cell imaging showed that reorganization and reassembly of actin microfilaments is dependent on microtubules following drug-induced depolymerization (49). Altered actin organization related to microtubule severing was not described yet. Here, we show that disturbed microtubule severing in the *ktn1-2* mutant might also have direct impact on the actin organization, which is mediated by increased abundances of MDP25 and profilin 1 but decreased abundance of ADF3. In fact, the equilibrium of profilins and ADFs directs the actin filaments to polymerization or depolymerization (50). MDP25 is a promising candidate potentially linking KATANIN 1 with actin microfilaments. Further targeted analyses would be beneficial to experimentally study interactions between katanin and ABPs.

Katanin Mutants Exerts Aberrant Nuclear Shape Likely Caused by Deregulation of WPP2 and HSC70–1—Roots of *fra2* mutant possess substantially decreased levels of WPP domain-containing protein 2 (WPP2). WPP2 is localized to the nuclear envelope in interphase cells and to immature cell plates during cytokinesis (39). This was consistent with changed nuclear shapes in both *KATANIN 1* mutants as revealed by DAPI staining. WPP proteins bind to WPP domain-interacting tail-anchored protein (WITs) and facilitate their nuclear envelope targeting (51). The same binding and targeting activity were assigned to heat shock cognate protein 70-1 (HSP70-1), which also interacts with WPPs (51). HSP70-1, unlike WPP2, showed an increased abundance in the *fra2* roots, suggesting an altered equilibrium in these two mechanisms of WIT nuclear targeting. WITs are constituents of plant Klarsicht/ANC-1/Syne-1 homology (KASH)–Sad1/UNC-84 (SUN) complex controlling nuclear morphology and movement (52). Recently, it was shown that WIT2 proteins interact and recruit myosin XI-i to the nuclear envelope and link KASH–SUN complexes with actin cytoskeleton (53), which is reorganized in the *KATANIN 1* mutants. Our results suggest that actin-dependent nuclear shape control in plants through WPP2 and WIT might be linked to microtubule severing by KATANIN 1.

Proteins Associated with Cell Plate Alterations in KATANIN 1 Mutants—In dividing cells, WPP2 might contribute to the emergence of obliquely oriented and misaligned cell plates in *KATANIN 1* mutants (this study and Ref. 21), which was tested here by co-immunolocalization of KNOLLE, a *bona fide* cell plate marker (34), and microtubules in the phragmoplast. Additionally, patellin 2 (down-regulated in the *ktn1-2* mutant roots) is a cell plate associated protein involved in the maturation of the cell plate (54). Recently, it was identified as a phosphorylation target of mitogen-activated protein kinase 4 (MPK4), whereas patellin phosphorylation by MPK4 altered its binding to phosphoinositides (55). The role of MPK4 in cell division is more complex, because it is also involved in phragmoplast formation through phosphorylation of phragmoplast-localized microtubule-associated protein MAP65-1 (9, 56–58). Together, WPP2 and patellin 2 may represent protein candidates co-regulated with KATANIN 1 during cytokinesis. In conclusion, phenotypes of *fra2* and *ktn1-2* mutants are likely determined by wider deregulation of developmentally important cytoskeletal and cell plate proteins.

Proteins Associated with Hormone Homeostasis in KATANIN 1 Mutants—It is well known that microtubule organization is responsive to plant hormones (40). KATANIN 1 was proposed as a mediator of GA- and ethylene-induced microtubule rearrangements in *Arabidopsis* (26). Mutant *lue1* exhibits increased *AtGA20ox1* expression levels, a key oxidase enzyme in the gibberellin biosynthesis. Hormonal responses of *lue1* to ethylene and gibberellins caused inappropriate cortical microtubule reorientation during cell growth (22). Other proteins regulating GA biosynthesis in *Arabidopsis*, like TSN1 and TSN2 and glycine-rich RNA-binding protein 7 (GRP7) (59, 60), were differentially abundant in *KATANIN 1* mutants. Although *TSN1* expression positively correlates with *AtGA20ox1* in *Arabidopsis* (59), *GRP7* appears to have a negative role (60).

In *fra2* we encountered also changed abundances of proteins involved in ethylene biosynthesis. Thus, 1-aminocyclopropane-1-carboxylate oxidase 2, catalyzing oxygen-dependent conversion of 1-aminocyclopropane-1-carboxylic acid to ethylene (61), was up-regulated. Moreover, 14-3-3-like protein GF14ω, found in Col-0 but not in the *KATANIN 1* mutants, was reported to control ethylene synthesis through down-regulation of ubiquitin ligases targeting 1-aminocyclopropane-1-carboxylate synthase for degradation (62). In contrast, enzymes controlling synthesis of ethylene precursor methionine, such as methionine synthase, *S*-adenosylmethionine synthetase 4, as well as 5-methyltetrahydropteroyltriglutamate-homocysteine methyltransferase (cobalamin-independent methionine synthase) (63), were down-regulated. Methionine is a precursor of *S*-adenosyl-L-methionine being a major methyl group donor for trans-methylation reactions (63). Adenosine kinase maintaining general

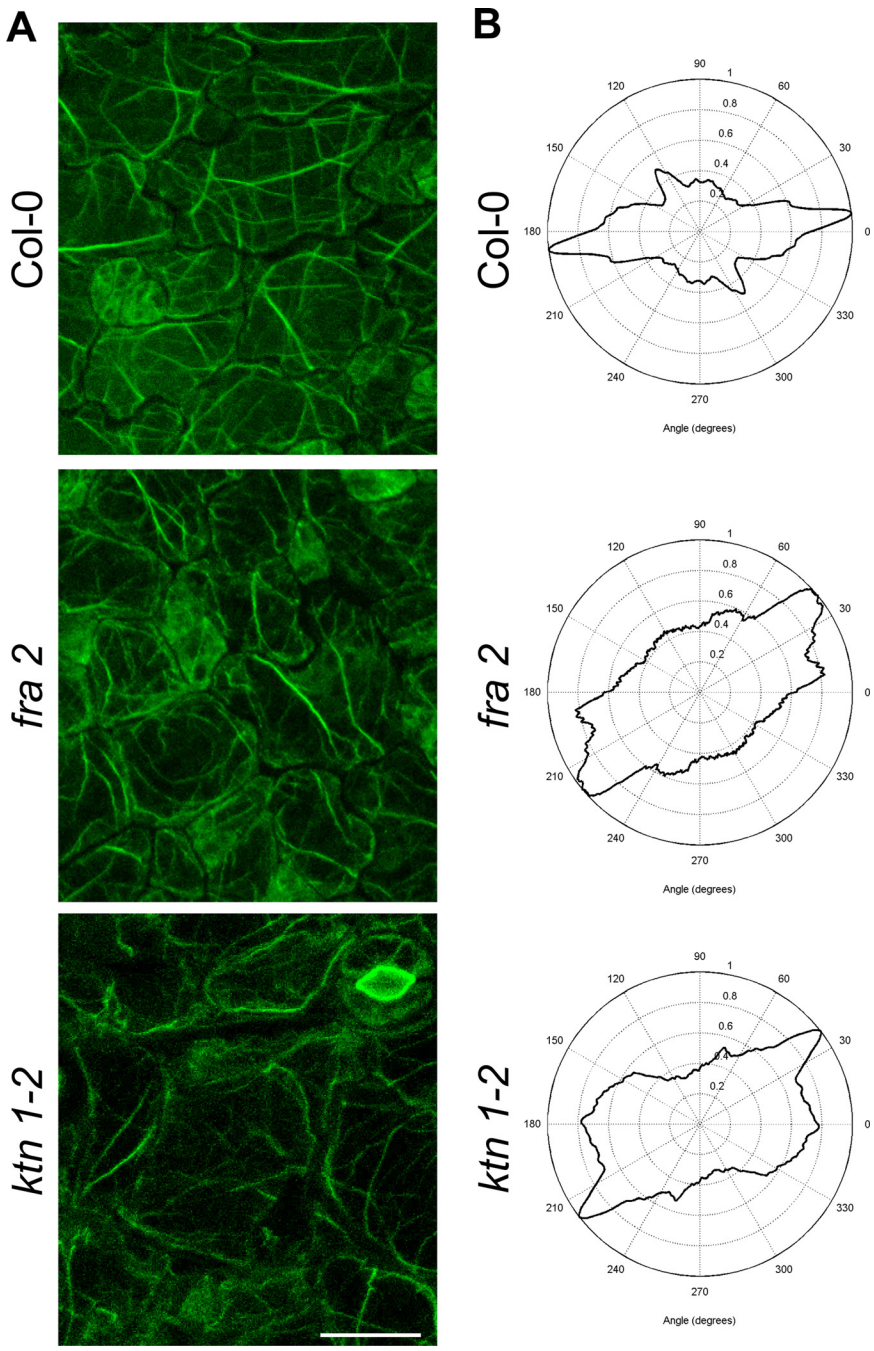

FIG. 10. **Filamentous actin (F-actin) organization in leaf epidermal cells of *Arabidopsis* wild type Col-0 and *KATANIN 1* mutants *fra2* and *ktn1-2*.** *A,* Alexa phalloidin was used for F-actin visualization. *B,* F-actin orientation and degree of isotropy analyzed by CytoSpectre software. Note reorientation of F-actin and higher anisotropy in both mutants in contrast to Col-0. Moreover, actin filaments are less prominent and look distorted in both mutants. *Bar,* 20 μm.

S-adenosyl-L-methionine-dependent methylation activities (64, 65) was up-regulated in the *fra2* mutant.

Our results point also to altered auxin homeostasis in *KATANIN 1* mutants. *S*-Alkyl-thiohydroximate lyase SUR1 (also known as SUPERROOT1), a protein involved in auxin biosynthesis, was detected only in wild-type roots suggesting down-regulation in the *KATANIN 1* mutants. Suppression of SUR1 results in heavy accumulation of auxin in *Arabidopsis* (66), and thus lower abundance in *KATANIN 1* mutants may indicate some defects in auxin homeostasis. This might be also influenced by pyruvate dehydrogenase E1 component subunit α-2, also called IAA-ALANINE-RESISTANT 4 (IAR4), which was strongly decreased in abundance in both *KATANIN 1* mutants, and it is implicated

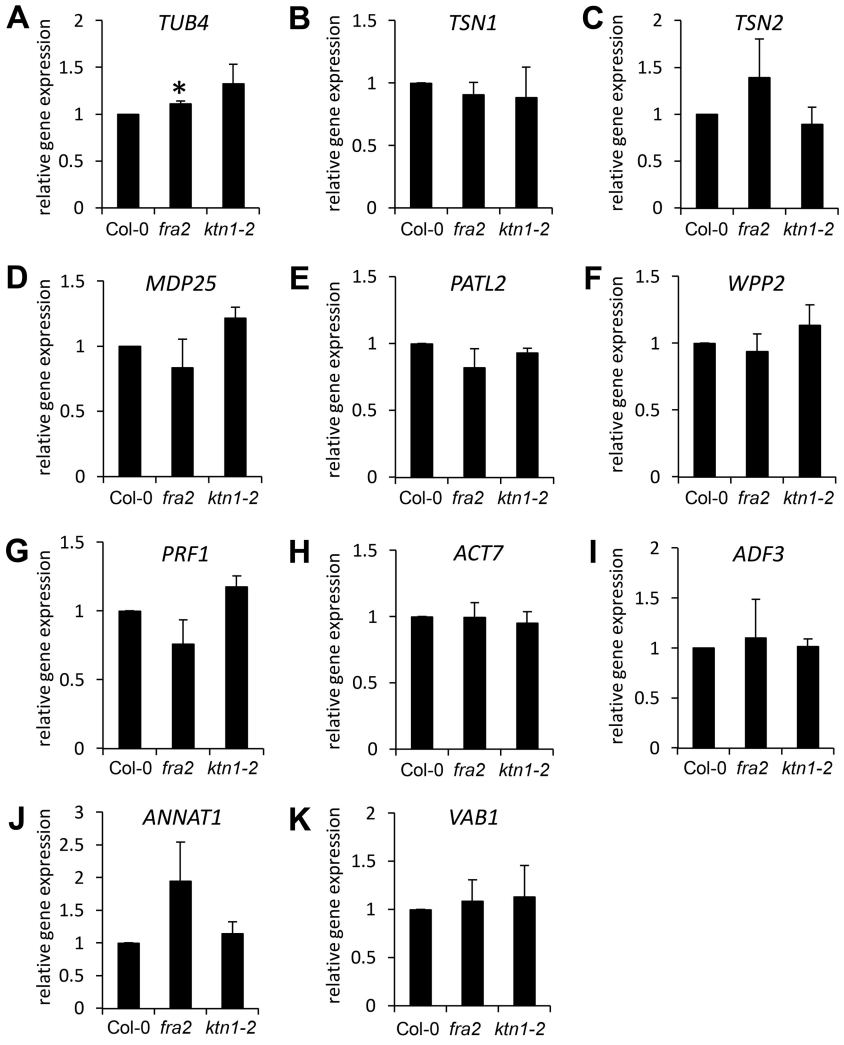

FIG. 11. **Quantitative expression levels of *TUBULIN β-4* (*TUB4; A*); *TUDOR-STAPHYLOCOCCAL NUCLEASE* (*TSN1; B*); *TSN2* (*C*); *MICROTUBULE-DESTABILIZING PROTEIN 25* (*MDP25; D*); *PATELLIN 2* (*PATL2; E*); *WPP DOMAIN-CONTAINING PROTEIN 2* (*WPP2; F*); and *PROFILIN 1* (*PRF1; G*) in roots, as well as *ACTIN 7* (*ACT7; H*); *ACTIN-DEPOLYMERIZING FACTOR 3 (ADF3; I*); *ANNEXIN 1* (*ANNAT1; J*); and *V-TYPE PROTON ATPASE SUBUNIT B1* (*VAB1*; *K*) in aerial parts of Col-0, *fra2,* and *ktn1-2.*** *Asterisk* in *A* indicates significant difference between *fra2* mutant and wild type at $p \leq 0.05$ according to Student's *t* test. *Error bars* represent standard deviations.

TABLE III

List of differentially abundant proteins in fra2 and ktn1-2 mutants (as compared with Col-0 wild type; $p \leq 0.05$), which are responsive to gibberellic acid as reported in transcriptomic study (86)

Accession	Protein name	Fold change *fra2 vs.* Col-0	Fold change *ktn1-2 vs.* Col-0	
gi18391066	2,3-Bisphosphoglycerate-independent phosphoglycerate mutase 1	1.78 (root)		Stomatal movements, pollen development (85)
gi334182565	Salt tolerance-related protein	0.57 (aerial parts)		Salt tolerance (87)
gi79313261	PYK10-binding protein 1	0.54 (root)	0.55 (root)	Defense (88)
gi15235401	Glutathione *S*-transferase F2	2.4 (root)	3.27 (root)	Stress tolerance (89)
gi79326500	Putative cinnamyl alcohol dehydrogenase 9	2.95 (aerial parts)		Lignification (90)

in IAA homeostasis (67, 68). Altogether, we show that, except for ethylene and GA, microtubule severing is likely linked to homeostasis of abscisic acid and auxin. The mechanism of hormonal regulation by KATANIN 1 is not known. One possible explanation is suggested by changes in enzymes responsible for methylation in the *KATANIN 1* mutants, because they have been shown to control hormone homeostasis in plants (69).

TABLE IV

List of differentially abundant proteins in fra2 and ktn1-2 mutants (as compared with Col-0 wild type; $p \leq 0.05$) containing GA-responsive element ACGTGTC (86) in their promoter sequence (1000 kb upstream of ATG)

Accession no.	Protein name	Position (upstream of ATG)	Fold change		Function
			fra2 vs. Col-0	*ktn1-2 vs.* Col-0	
gi334183935	Dehydrin ERD14	843−850	0.22 (aerial parts)	0.52 (aerial parts)	Stress response (91)
gi15233111	Cysteine synthase C1	472−479	3.55 (root)	2.61 (root)	Defense (92)
gi79326500	Putative cinnamyl alcohol dehydrogenase 9	428−435	2.95 (aerial parts)		Lignification (90)
gi18406229	TRAF-like protein	131−138		1.45 (roots)	Unknown
gi15227259	Cyclophilin ROC3	128−135		0.43 (roots)	Defense (93)
gi15234637	Photosystem II subunit Q-2	149−156		1.45 (aerial parts)	Photosystem II assembly (94)
gi15238217	Sulfite reductase	89−96		0.43 (roots)	Sulfate assimilation, growth and development (95)

TABLE V

List of differentially abundant proteins in fra2 and ktn1-2 mutants (as compared with Col-0 wild type; $p \leq 0.05$) containing abscisic acid-responsive element (ABRE) in their promoter sequence (1000 kb upstream of ATG)

ABRE	Accession no.	Protein name	Position (upstream of ATG)	Fold change		Function
				fra2 vs Col-0	*ktn1-2* vs Col-0	
ACACGTGTC	gi334183935	Dehydrin ERD14	571−562	0.22 (aerial parts)	0.52 (aerial parts)	Stress response (91)
ACACGTGGC	gi15220216	Annexin 1	49−40	1.67 (aerial parts)	0.55 (aerial parts)	Actin-binding, calcium signaling (96, 97)
ACACGTGTA	gi15220854	Alkenal/one oxidoreductase	339−330	0.52 (aerial parts)		Removal of reactive carbonyls (98)
	gi15228498	UDP-glucose pyrophosphorylase 1	74−65	1.43 (roots)		Cellulose and callose formation, growth, development (99, 100)
	gi30687411	Dihydrolipoamide succinyltransferase	56−47	*fra2* unique (aerial parts)		Unknown
ACACGTGTT	gi15233272	Triose-phosphate isomerase	928−919	1.49 (roots)		Glycolysis, gluconeogenesis (101)
CCACGTGGC	gi15242459	Mitochondrial HSO70 2	79−70	1.66 (roots)		
CCACGTGTT	gi79326500	Putative cinnamyl alcohol dehydrogenase 9	959−950	2.95 (aerial parts)		Lignification (90)
CCACGTGTC	gi15227259	Cyclophilin ROC3	75−66		0.43 (roots)	Defense (93)
	gi15234637	Photosystem II subunit Q-2	78−69		1.45 (aerial parts)	Photosystem II organization (94)
CTACGTGTC	gi18406229	TRAF-like protein	155−146		1.45 (roots)	Unknown
GCACGTGTC	gi15238217	Sulfite reductase	91−82		0.43 (roots)	Sulfate assimilation , growth and development (95)
CTACGTGTT	gi15242451	AIG2-like protein	62−53		2.72 (roots)	Unknown
CCACGTGTG	gi18417239	Photosystem II reaction center PSB28 protein	164−155		2.79 (aerial parts)	Photosystem II assembly (102)

Because of the substantial impact on agriculturally important crop traits, cytoskeleton and cytoskeleton-associated proteins serve as perspective subjects of genetic engineering for biotechnological applications (70). Our study strengthens this view and provides proteome framework for developmental defects related to KATANIN 1 function. Thus, genetic modification of *KATANIN 1* may be considered as a tool to modify plant growth and development.

In conclusion, genetic disruption of microtubule severing in *fra2* and *ktn1-2* mutants shows a strong impact on the abundance of tubulins, MAP, actin, and ABPs and on the organization of both microtubules and actin filaments. Thus, our study opens a door to investigate these new aspects of feedback microtubule control and cross-talk between microtubules and actin cytoskeleton in plants involving KATANIN 1.

Acknowledgments—We thank George Komis and Miroslav Ovečka for critical reading of the manuscript and George Komis for help with CytoSpectre software. Tony Arick created computer script to sum ion intensities for multiple samples. We thank Dr. Masayoshi Nakamura for kindly providing *ktn1-2* seeds and Drs. Ioannis Adamakis and Emanuel Panteris for providing *fra2* seeds. We also thank Dr. Panagiotis Moschou and Prof. Gerd Juergens for kindly providing anti-TSN1/2 and anti-KNOLLE primary antibodies. The mass spectrometry proteomics analysis was performed at the Institute for Genomics, Biocomputing and Biotechnology, Mississippi State University, with partial support from Mississippi Agriculture and Forestry Experimental Station.

DATA AVAILABILITY

The mass spectrometry proteomics data have been deposited to the ProteomeXchange Consortium via the PRIDE (71) partner repository with the dataset identifier PXD005917 (http://www.ebi.ac.uk/pride/archive/). In addition to ".raw" data files, the ".msf" results files areavailable to download. They can be viewed free of charge using Proteome Discoverer demo/viewer (https://portal.thermo-brims.com/).

* This work was supported by Grant 15-19284S from the Czech Science Foundation GAČR and National Institutes of Health-INBRE Award 4P20GM103476-15. The authors declare that they have no conflicts of interest with the contents of this article. The content is solely the responsibility of the authors and does not necessarily represent the official views of the National Institutes of Health.

S This article contains supplemental material.

¶ Both authors contributed equally to this work.
‖ To whom correspondence should be addressed: Centre of the Region Haná for Biotechnological and Agricultural Research, Faculty of Science, Palacký University, Šlechtitelů 27, 783 71 Olomouc, Czech Republic. Tel.: 00420585634978; E-mail: jozef.samaj@upol.cz.

REFERENCES

1. Cyr, R. J. (1994) Microtubules in plant morphogenesis: role of the cortical array. *Annu. Rev. Cell Biol.* **10,** 153–180
2. Kost, B., Mathur, J., and Chua, N.-H. (1999) Cytoskeleton in plant development. *Curr. Opin. Plant Biol.* **2,** 462–470
3. Goddard, R. H., Wick, S. M., Silflow, C. D., and Snustad, D. P. (1994) Microtubule components of the plant cell cytoskeleton. *Plant Physiol.* **104,** 1–6
4. Wasteneys, G. O., and Ambrose, J. C. (2009) Spatial organization of plant cortical microtubules: close encounters of the 2D kind. *Trends Cell Biol.* **19,** 62–71
5. Sedbrook, J. C., and Kaloriti, D. (2008) Microtubules, MAPs and plant directional cell expansion. *Trends Plant Sci.* **13,** 303–310
6. Hamada, T. (2007) Microtubule-associated proteins in higher plants. *J. Plant Res.* **120,** 79–98
7. Gardiner, J. (2013) The evolution and diversification of plant microtubule-associated proteins. *Plant J.* **75,** 219–229
8. Šamajová, O., Komis, G., and Šamaj, J. (2013) Emerging topics in the cell biology of mitogen-activated protein kinases. *Trends Plant Sci.* **18,** 140–148
9. Beck, M., Komis, G., Müller, J., Menzel, D., and Samaj, J. (2010) *Arabidopsis* homologs of nucleus- and phragmoplast-localized kinase 2 and 3 and mitogen-activated protein kinase 4 are essential for microtubule organization. *Plant Cell* **22,** 755–771
10. Müller, J., Beck, M., Mettbach, U., Komis, G., Hause, G., Menzel, D., and Samaj, J. (2010) *Arabidopsis* MPK6 is involved in cell division plane control during early root development, and localizes to the pre-prophase band, phragmoplast, trans-Golgi network and plasma membrane. *Plant J.* **61,** 234–248
11. Komatsu, S., Yang, G., Khan, M., Onodera, H., Toki, S., and Yamaguchi, M. (2007) Over-expression of calcium-dependent protein kinase 13 and calreticulin interacting protein 1 confers cold tolerance on rice plants. *Mol. Genet. Genomics* **277,** 713–723
12. Yalovsky, S., Bloch, D., Sorek, N., and Kost, B. (2008) Regulation of membrane trafficking, cytoskeleton dynamics, and cell polarity by ROP/RAC GTPases. *Plant Physiol.* **147,** 1527–1543
13. Zhang, Q., Lin, F., Mao, T., Nie, J., Yan, M., Yuan, M., and Zhang, W. (2012) Phosphatidic acid regulates microtubule organization by interacting with MAP65–1 in response to salt stress in *Arabidopsis. Plant Cell* **24,** 4555–4576
14. Hartman, J. J., Mahr, J., McNally, K., Okawa, K., Iwamatsu, A., Thomas, S., Cheesman, S., Heuser, J., Vale, R. D., and McNally, F. J. (1998) Katanin, a microtubule-severing protein, is a novel AAA ATPase that targets to the centrosome using a WD40-containing subunit. *Cell* **93,** 277–287
15. Stoppin-Mellet, V., Gaillard, J., Timmers, T., Neumann, E., Conway, J., and Vantard, M. (2007) *Arabidopsis* katanin binds microtubules using a multimeric microtubule-binding domain. *Plant Physiol. Biochem.* **45,** 867–877
16. Nakamura, M. (2015) Microtubule nucleating and severing enzymes for modifying microtubule array organization and cell morphogenesis in response to environmental cues. *New Phytol.* **205,** 1022–1027
17. Stoppin-Mellet, V., Gaillard, J., and Vantard, M. (2006) Katanin's severing activity favors bundling of cortical microtubules in plants. *Plant J.* **46,** 1009–1017
18. Wightman, R., Chomicki, G., Kumar, M., Carr, P., and Turner, S. R. (2013) SPIRAL2 determines plant microtubule organization by modulating microtubule severing. *Curr. Biol.* **23,** 1902–1907
19. Lin, D., Cao, L., Zhou, Z., Zhu, L., Ehrhardt, D., Yang, Z., and Fu, Y. (2013) Rho GTPase signaling activates microtubule severing to promote microtubule ordering in *Arabidopsis*. *Curr. Biol.* **23,** 290–297
20. Bichet, A., Desnos, T., Turner, S., Grandjean, O., and Höfte, H. (2001) BOTERO1 is required for normal orientation of cortical microtubules and anisotropic cell expansion in *Arabidopsis*. *Plant J.* **25,** 137–148
21. Burk, D. H., Liu, B., Zhong, R., Morrison, W. H., and Ye, Z. H. (2001) A katanin-like protein regulates normal cell wall biosynthesis and cell elongation. *Plant Cell* **13,** 807–827
22. Meier, C., Bouquin, T., Nielsen, M. E., Raventos, D., Mattsson, O., Rocher, A., Schomburg, F., Amasino, R. M., and Mundy, J. (2001) Gibberellin response mutants identified by luciferase imaging. *Plant J.* **25,** 509–519
23. Luptovčiak, I., Samakovli, D., Komis, G., and Šamaj, J. (2017) KATANIN 1 is essential for embryogenesis and seed formation in *Arabidopsis*. *Front. Plant Sci.* **8,** 728
24. Panteris, E., Adamakis, I.-D., Voulgari, G., and Papadopoulou, G. (2011) A role for katanin in plant cell division: microtubule organization in dividing root cells of fra2 and lue1 *Arabidopsis thaliana* mutants. *Cytoskeleton* **68,** 401–413
25. Komis, G., Luptovčiak, I., Ovečka, M., Samakovli, D., Šamajová, Oand Šamaj, J. (2017) Katanin effects on dynamics of cortical microtubules and mitotic arrays in *Arabidopsis thaliana* revealed by advanced live-cell imaging. *Front. Plant Sci.* **8,** 866
26. Bouquin, T., Mattsson, O., Naested, H., Foster, R., and Mundy, J. (2003) The *Arabidopsis* lue1 mutant defines a katanin p60 ortholog involved in hormonal control of microtubule orientation during cell growth. *J. Cell Sci.* **116,** 791–801
27. Vasconcelos, E. J. R., Pacheco, A. C. L., Gouveia, J. J. S., Araujo, F. F., Diniz, M. C., Kamimura, M. T., Costa, M. P., Maggioni, R., Araujo-Filho, R., Costa, R. B., and de Oliveira, D. M. (2007) *Profilins, Formins and Katanins as Flagellar Proteins of Leishmania spp.: A Genome-based, Multi-step Bioinformatics-driven Description*. *October 14–17, 2007, Boston, MA.* 2007 IEEE 7th International Symposium on BioInformatics and BioEngineering, pp. 880–887, IEEE, New York
28. Cheung, K., Senese, S., Kuang, J., Bui, N., Ongpipattanakul, C., Gholkar, A., Cohn, W., Capri, J., Whitelegge, J. P., and Torres, J. Z. (2016) Proteomic analysis of the mammalian Katanin Family of microtubule-severing enzymes defines Katanin p80 subunit B-like 1 (KATNBL1) as a regulator of mammalian Katanin microtubule-severing. *Mol. Cell. Proteomics* **15,** 1658–1669
29. Hajduch, M., Ganapathy, A., Stein, J. W., and Thelen, J. J. (2005) A systematic proteomic study of seed filling in soybean. Establishment of high-resolution two-dimensional reference maps, expression profiles, and an interactive proteome database. *Plant Physiol.* **137,** 1397–1419
30. Conesa, A., and Götz, S. (2008) Blast2GO: A comprehensive suite for functional analysis in plant genomics. *Int. J. Plant Genomics* **2008,** 619832
31. Szklarczyk, D., Franceschini, A., Wyder, S., Forslund, K., Heller, D., Huerta-Cepas, J., Simonovic, M., Roth, A., Santos, A., Tsafou, K. P., Kuhn, M., Bork, P., Jensen, L. J., and von Mering, C. (2015) STRING v10: protein-protein interaction networks, integrated over the tree of life. *Nucleic Acids Res.* **43,** D447–D452
32. Gutierrez-Beltran, E., Moschou, P. N., Smertenko, A. P., and Bozhkov, P. V. (2015) Tudor staphylococcal nuclease links formation of stress granules and processing bodies with mRNA catabolism in *Arabidopsis*. *Plant Cell* **27,** 926–943
33. Smékalová, V., Luptovčiak, I., Komis, G., Šamajová, O., Ovečka, M., Doskočilová, A., Takáč, T., Vadovič, P., Novák, O., Pechan, T., Ziemann, A., Košútová, P., and Šamaj, J. (2014) Involvement of YODA and mitogen activated protein kinase 6 in *Arabidopsis* post-embryogenic root development through auxin up-regulation and cell division plane orientation. *New Phytol.* **203,** 1175–1193
34. Lauber, M. H., Waizenegger, I., Steinmann, T., Schwarz, H., Mayer, U., Hwang, I., Lukowitz, W., and Jürgens, G. (1997) The *Arabidopsis* KNOLLE protein is a cytokinesis-specific syntaxin. *J. Cell Biol.* **139,** 1485–1493
35. Kartasalo, K., Pölönen, R.-P., Ojala, M., Rasku, J., Lekkala, J., Aalto-Setälä, K., and Kallio, P. (2015) CytoSpectre: a tool for spectral analysis of oriented structures on cellular and subcellular levels. *BMC Bioinformatics* **16,** 344
36. Panteris, E., Apostolakos, P., and Galatis, B. (2006) Cytoskeletal asymmetry in *Zea mays* subsidiary cell mother cells: a monopolar prophase microtubule half-spindle anchors the nucleus to its polar position. *Cell Motil. Cytoskeleton* **63,** 696–709
37. Li, J., Wang, X., Qin, T., Zhang, Y., Liu, X., Sun, J., Zhou, Y., Zhu, L., Zhang, Z., Yuan, M., and Mao, T. (2011) MDP25, a novel calcium regulatory protein, mediates hypocotyl cell elongation by destabilizing cortical microtubules in *Arabidopsis*. *Plant Cell* **23,** 4411–4427

38. Qin, T., Liu, X., Li, J., Sun, J., Song, L., and Mao, T. (2014) *Arabidopsis* microtubule-destabilizing protein 25 functions in pollen tube growth by severing actin filaments. *Plant Cell* **26,** 325–339
39. Patel, S., Rose, A., Meulia, T., Dixit, R., Cyr, R. J., and Meier, I. (2004) *Arabidopsis* WPP-domain proteins are developmentally associated with the nuclear envelope and promote cell division. *Plant Cell* **16,** 3260–3273
40. Shibaoka, H. (1994) Plant hormone-induced changes in the orientation of cortical microtubules–alterations in the cross-linking between microtubules and the plasma-membrane. *Annu. Rev. Plant Physiol. Plant Mol. Biol.* **45,** 527–544
41. Gallardo, K., Job, C., Groot, S. P., Puype, M., Demol, H., Vandekerckhove, J., and Job, D. (2002) Proteomics of *Arabidopsis* seed germination. A comparative study of wild-type and gibberellin-deficient seeds. *Plant Physiol.* **129,** 823–837
42. Hamada, T., Nagasaki-Takeuchi, N., Kato, T., Fujiwara, M., Sonobe, S., Fukao, Y., and Hashimoto, T. (2013) Purification and characterization of novel microtubule-associated proteins from *Arabidopsis* cell suspension cultures. *Plant Physiol.* **163,** 1804–1816
43. Szymanski, W. G., Zauber, H., Erban, A., Gorka, M., Wu, X. N., and Schulze, W. X. (2015) Cytoskeletal components define protein location to membrane microdomains. *Mol. Cell. Proteomics* **14,** 2493–2509
44. Takáč, T., Bekešová, S., and Šamaj, J. (2017) Actin depolymerization-induced changes in proteome of *Arabidopsis* roots. *J. Proteomics* **153,** 89–99
45. de Graauw, M., Tijdens, I., Smeets, M. B., Hensbergen, P. J., Deelder, A. M., and van de Water, B. (2008) Annexin A2 phosphorylation mediates cell scattering and branching morphogenesis via cofilin activation. *Mol. Cell. Biol.* **28,** 1029–1040
46. Blancaflor, E. B. (2000) Cortical actin filaments potentially interact with cortical microtubules in regulating polarity of cell expansion in primary roots of maize (*Zea mays* L.). *J. Plant Growth Regul.* **19,** 406–414
47. Collings, D. A. (2008) in *Plant Microtubules–Development and Flexibility* (Nick, P., ed) pp. 47–82, Springer-Verlag, Berlin
48. Havelková, L., Nanda, G., Martinek, J., Bellinvia, E., Sikorová, L., Šlajcherová, K., Seifertová, D., Fischer, L., Fišerová, J., Petrášek, J., and Schwarzerová, K. (2015) Arp2/3 complex subunit ARPC2 binds to microtubules. *Plant Sci.* **241,** 96–108
49. Sampathkumar, A., Lindeboom, J. J., Debolt, S., Gutierrez, R., Ehrhardt, D. W., Ketelaar, T., and Persson, S. (2011) Live cell imaging reveals structural associations between the actin and microtubule cytoskeleton in *Arabidopsis*. *Plant Cell* **23,** 2302–2313
50. Li, J., Blanchoin, L., and Staiger, C. J. (2015) Signaling to actin stochastic dynamics. *Annu. Rev. Plant Biol.* **66,** 415–440
51. Brkljacic, J., Zhao, Q., and Meier, I. (2009) WPP-domain proteins mimic the activity of the HSC70–1 chaperone in preventing mistargeting of RanGAP1-anchoring protein WIT1. *Plant Physiol.* **151,** 142–154
52. Zhou, X., Graumann, K., Evans, D. E., and Meier, I. (2012) Novel plant SUN-KASH bridges are involved in RanGAP anchoring and nuclear shape determination. *J. Cell Biol.* **196,** 203–211
53. Zhou, X., Groves, N. R., and Meier, I. (2015) Plant nuclear shape is independently determined by the SUN-WIP-WIT2-myosin XI-i complex and CRWN1. *Nucleus* **6,** 144–153
54. Peterman, T. K., Ohol, Y. M., McReynolds, L. J., and Luna, E. J. (2004) Patellin1, a novel Sec14-like protein, localizes to the cell plate and binds phosphoinositides. *Plant Physiol.* **136,** 3080–3094
55. Suzuki, T., Matsushima, C., Nishimura, S., Higashiyama, T., Sasabe, M., and Machida, Y. (2016) Identification of phosphoinositide-binding protein PATELLIN2 as a substrate of *Arabidopsis* MPK4 MAP kinase during septum formation in cytokinesis. *Plant Cell Physiol.* **57,** 1744–1755
56. Smertenko, A. P., Chang, H.-Y., Sonobe, S., Fenyk, S. I., Weingartner, M., Bögre, L., and Hussey, P. J. (2006) Control of the AtMAP65–1 interaction with microtubules through the cell cycle. *J. Cell Sci.* **119,** 3227–3237
57. Kosetsu, K., Matsunaga, S., Nakagami, H., Colcombet, J., Sasabe, M., Soyano, T., Takahashi, Y., Hirt, H., and Machida, Y. (2010) The MAP kinase MPK4 is required for cytokinesis in *Arabidopsis thaliana*. *Plant Cell* **22,** 3778–3790
58. Beck, M., Komis, G., Ziemann, A., Menzel, D., and Samaj, J. (2011) Mitogen-activated protein kinase 4 is involved in the regulation of mitotic and cytokinetic microtubule transitions in *Arabidopsis thaliana*. *New Phytol.* **189,** 1069–1083
59. Yan, C., Yan, Z., Wang, Y., Yan, X., and Han, Y. (2014) Tudor-SN, a component of stress granules, regulates growth under salt stress by modulating GA20ox3 mRNA levels in *Arabidopsis*. *J. Exp. Bot.* **65,** 5933–5944
60. Löhr, B., Streitner, C., Steffen, A., Lange, T., and Staiger, D. (2014) A glycine-rich RNA-binding protein affects gibberellin biosynthesis in *Arabidopsis*. *Mol. Biol. Rep.* **41,** 439–445
61. Ruduś, I., Sasiak, M., and Kępczyński, J. (2013) Regulation of ethylene biosynthesis at the level of 1-aminocyclopropane-1-carboxylate oxidase (ACO) gene. *Acta Physiol. Plant.* **35,** 295–307
62. Yoon, G. M., and Kieber, J. J. (2013) 14-3-3 regulates 1-aminocyclopropane-1-carboxylate synthase protein turnover in *Arabidopsis*. *Plant Cell* **25,** 1016–1028
63. Ravanel, S., Gakière, B., Job, D., and Douce, R. (1998) The specific features of methionine biosynthesis and metabolism in plants. *Proc. Natl. Acad. Sci. U.S.A.* **95,** 7805–7812
64. Moffatt, B. A., Stevens, Y. Y., Allen, M. S., Snider, J. D., Pereira, L. A., Todorova, M. I., Summers, P. S., Weretilnyk, E. A., Martin-McCaffrey, L., and Wagner, C. (2002) Adenosine kinase deficiency is associated with developmental abnormalities and reduced transmethylation. *Plant Physiol.* **128,** 812–821
65. Weretilnyk, E. A., Alexander, K. J., Drebenstedt, M., Snider, J. D., Summers, P. S., and Moffatt, B. A. (2001) Maintaining methylation activities during salt stress. The involvement of adenosine kinase. *Plant Physiol.* **125,** 856–865
66. Boerjan, W., Cervera, M. T., Delarue, M., Beeckman, T., Dewitte, W., Bellini, C., Caboche, M., Van Onckelen, H., Van Montagu, M., and Inzé, D. (1995) Superroot, a recessive mutation in *Arabidopsis*, confers auxin overproduction. *Plant Cell* **7,** 1405–1419
67. LeClere, S., Rampey, R. A., and Bartel, B. (2004) IAR4, a gene required for auxin conjugate sensitivity in *Arabidopsis*, encodes a pyruvate dehydrogenase E1α homolog. *Plant Physiol.* **135,** 989–999
68. Quint, M., Barkawi, L. S., Fan, K.-T., Cohen, J. D., and Gray, W. M. (2009) *Arabidopsis* IAR4 modulates auxin response by regulating auxin homeostasis. *Plant Physiol.* **150,** 748–758
69. Westfall, C. S., Muehler, A. M., and Jez, J. M. (2013) Enzyme action in the regulation of plant hormone responses. *J. Biol. Chem.* **288,** 19304–19311
70. Komis, G., Luptovciak, I., Doskocilova, A., and Samaj, J. (2015) Biotechnological aspects of cytoskeletal regulation in plants. *Biotechnol. Adv.* **33,** 1043–1062
71. Vizcaíno, J. A., Csordas, A., del-Toro, N., Dianes, J. A., Griss, J., Lavidas, I., Mayer, G., Perez-Riverol, Y., Reisinger, F., Ternent, T., Xu, Q.-W., Wang, R., and Hermjakob, H. (2016) 2016 update of the PRIDE database and its related tools. *Nucleic Acids Res.* **44,** D447–D456
72. Dalal, J., Lewis, D. R., Tietz, O., Brown, E. M., Brown, C. S., Palme, K., Muday, G. K., and Sederoff, H. W. (2016) ROSY1, a novel regulator of gravitropic response is a stigmasterol binding protein. *J. Plant Physiol.* **196,** 28–40
73. Nishimura, N., Sarkeshik, A., Nito, K., Park, S.-Y., Wang, A., Carvalho, P. C., Lee, S., Caddell, D. F., Cutler, S. R., Chory, J., Yates, J. R., and Schroeder, J. I. (2010) PYR/PYL/RCAR family members are major *in vivo* ABI1 protein phosphatase 2C-interacting proteins in *Arabidopsis*. *Plant J.* **61,** 290–299
74. Sjögren, L. L., MacDonald, T. M., Sutinen, S., and Clarke, A. K. (2004) Inactivation of the clpC1 gene encoding a chloroplast Hsp100 molecular chaperone causes growth retardation, leaf chlorosis, lower photosynthetic activity, and a specific reduction in photosystem content. *Plant Physiol.* **136,** 4114–4126
75. Weijers, D., Franke-van Dijk, M., Vencken, R. J., Quint, A., Hooykaas, P., and Offringa, R. (2001) An *Arabidopsis* minute-like phenotype caused by a semi-dominant mutation in a RIBOSOMAL PROTEIN S5 gene. *Development* **128,** 4289–4299
76. Romani, I., Tadini, L., Rossi, F., Masiero, S., Pribil, M., Jahns, P., Kater, M., Leister, D., and Pesaresi, P. (2012) Versatile roles of *Arabidopsis* plastid ribosomal proteins in plant growth and development. *Plant J.* **72,** 922–934
77. De Castro, R. D., Zheng, X., Bergervoet, J., De Vos, C., and Bino, R. J. (1995) β-Tubulin accumulation and DNA replication in imbibing tomato seeds. *Plant Physiol.* **109,** 499–504
78. Sundström, J. F., Vaculova, A., Smertenko, A. P., Savenkov, E. I., Golovko, A., Minina, E., Tiwari, B. S., Rodriguez-Nieto, S., Zamyatnin,

A. A., Jr., Välineva, T., Saarikettu, J., Frilander, M. J., Suarez, M. F., Zavialov, A., Ståhl, U., *et al.* (2009) Tudor staphylococcal nuclease is an evolutionarily conserved component of the programmed cell death degradome. *Nat. Cell Biol.* **11,** 1347–1354
79. Ramachandran, S., Christensen, H. E., Ishimaru, Y., Dong, C. H., Chao-Ming, W., Cleary, A. L., and Chua, N. H. (2000) Profilin plays a role in cell elongation, cell shape maintenance, and flowering in *Arabidopsis*. *Plant Physiol.* **124,** 1637–1647
80. Sheoran, I. S., Olson, D. J., Ross, A. R., and Sawhney, V. K. (2005) Proteome analysis of embryo and endosperm from germinating tomato seeds. *Proteomics* **5,** 3752–3764
81. Augustine, R. C., Vidali, L., Kleinman, K. P., and Bezanilla, M. (2008) Actin-depolymerizing factor is essential for viability in plants, and its phosphoregulation is important for tip growth. *Plant J.* **54,** 863–875
82. Gilliland, L. U., Pawloski, L. C., Kandasamy, M. K., and Meagher, R. B. (2003) *Arabidopsis* actin gene ACT7 plays an essential role in germination and root growth. *Plant J.* **33,** 319–328
83. Gallardo, K., Job, C., Groot, S. P., Puype, M., Demol, H., Vandekerckhove, J., and Job, D. (2001) Proteomic analysis of *Arabidopsis* seed germination and priming. *Plant Physiol.* **126,** 835–848
84. Ma, B., Qian, D., Nan, Q., Tan, C., An, L., and Xiang, Y. (2012) *Arabidopsis* vacuolar H^+-ATPase (V-ATPase) B subunits are involved in actin cytoskeleton remodeling via binding to, bundling, and stabilizing F-actin. *J. Biol. Chem.* **287,** 19008–19017
85. Zhao, Z., and Assmann, S. M. (2011) The glycolytic enzyme, phosphoglycerate mutase, has critical roles in stomatal movement, vegetative growth, and pollen production in *Arabidopsis thaliana*. *J. Exp. Bot.* **62,** 5179–5189
86. Ogawa, M., Hanada, A., Yamauchi, Y., Kuwahara, A., Kamiya, Y., and Yamaguchi, S. (2003) Gibberellin biosynthesis and response during *Arabidopsis* seed germination. *Plant Cell* **15,** 1591–1604
87. Du, J., Huang, Y.-P., Xi, J., Cao, M.-J., Ni, W.-S., Chen, X., Zhu, J.-K., Oliver, D. J., and Xiang, C.-B. (2008) Functional gene-mining for salt-tolerance genes with the power of *Arabidopsis*. *Plant J.* **56,** 653–664
88. Matsushima, R., Fukao, Y., Nishimura, M., and Hara-Nishimura, I. (2004) NAI1 gene encodes a basic-helix-loop-helix-type putative transcription factor that regulates the formation of an endoplasmic reticulum-derived structure, the ER body. *Plant Cell* **16,** 1536–1549
89. Lee, S.-H., Li, C.-W., Koh, K. W., Chuang, H.-Y., Chen, Y.-R., Lin, C.-S., and Chan, M.-T. (2014) MSRB7 reverses oxidation of GSTF2/3 to confer tolerance of *Arabidopsis thaliana* to oxidative stress. *J. Exp. Bot.* **65,** 5049–5062
90. Eudes, A., Pollet, B., Sibout, R., Do, C.-T., Séguin, A., Lapierre, C., and Jouanin, L. (2006) Evidence for a role of AtCAD 1 in lignification of elongating stems of *Arabidopsis thaliana*. *Planta* **225,** 23–39
91. Kovacs, D., Kalmar, E., Torok, Z., and Tompa, P. (2008) Chaperone activity of ERD10 and ERD14, two disordered stress-related plant proteins. *Plant Physiol.* **147,** 381–390
92. García, I., Rosas, T., Bejarano, E. R., Gotor, C., and Romero, L. C. (2013) Transient transcriptional regulation of the CYS-C1 gene and cyanide accumulation upon pathogen infection in the plant immune response. *Plant Physiol.* **162,** 2015–2027
93. Pogorelko, G. V., Mokryakova, M., Fursova, O. V., Abdeeva, I., Piruzian, E. S., and Bruskin, S. A. (2014) Characterization of three *Arabidopsis thaliana* immunophilin genes involved in the plant defense response against *Pseudomonas syringae*. *Gene* **538,** 12–22
94. Allahverdiyeva, Y., Suorsa, M., Rossi, F., Pavesi, A., Kater, M. M., Antonacci, A., Tadini, L., Pribil, M., Schneider, A., Wanner, G., Leister, D., Aro, E.-M., Barbato, R., and Pesaresi, P. (2013) *Arabidopsis* plants lacking PsbQ and PsbR subunits of the oxygen-evolving complex show altered PSII super-complex organization and short-term adaptive mechanisms. *Plant J.* **75,** 671–684
95. Khan, M. S., Haas, F. H., Samami, A. A., Gholami, A. M., Bauer, A., Fellenberg, K., Reichelt, M., Hänsch, R., Mendel, R. R., Meyer, A. J., Wirtz, M., and Hell, R. (2010) Sulfite reductase defines a newly discovered bottleneck for assimilatory sulfate reduction and is essential for growth and development in *Arabidopsis thaliana*. *Plant Cell* **22,** 1216–1231
96. Hu, S., Brady, S. R., Kovar, D. R., Staiger, C. J., Clark, G. B., Roux, S. J., and Muday, G. K. (2000) Technical advance: identification of plant actin-binding proteins by F-actin affinity chromatography. *Plant J.* **24,** 127–137
97. Davies, J. M. (2014) Annexin-mediated calcium signalling in plants. *Plants* **3,** 128–140
98. Takagi, D., Ifuku, K., Ikeda, K., Inoue, K. I., Park, P., Tamoi, M., Inoue, H., Sakamoto, K., Saito, R., and Miyake, C. (2016) Suppression of chloroplastic alkenal/one oxidoreductase represses the carbon catabolic pathway in *Arabidopsis* leaves during night. *Plant Physiol.* **170,** 2024–2039
99. Meng, M., Geisler, M., Johansson, H., Harholt, J., Scheller, H. V., Mellerowicz, E. J., and Kleczkowski, L. A. (2009) UDP-glucose pyrophosphorylase is not rate limiting, but is essential in *Arabidopsis*. *Plant Cell Physiol.* **50,** 998–1011
100. Park, J.-I., Ishimizu, T., Suwabe, K., Sudo, K., Masuko, H., Hakozaki, H., Nou, I.-S., Suzuki, G., and Watanabe, M. (2010) UDP-glucose pyrophosphorylase is rate limiting in vegetative and reproductive phases in *Arabidopsis thaliana*. *Plant Cell Physiol.* **51,** 981–996
101. López-Castillo, L. M., Jiménez-Sandoval, P., Baruch-Torres, N., Trasviña-Arenas, C. H., Díaz-Quezada, C., Lara-González, S., Winkler, R., and Brieba, L. G. (2016) Structural basis for redox regulation of cytoplasmic and chloroplastic triosephosphate isomerases from *Arabidopsis thaliana*. *Front. Plant Sci.* **7,** 1817
102. Mabbitt, P. D., Wilbanks, S. M., and Eaton-Rye, J. J. (2014) Structure and function of the hydrophilic Photosystem II assembly proteins: Psb27, Psb28 and Ycf48. *Plant Physiol. Biochem.* **81,** 96–107